# DETERMINATION OF STRESSES IN GROUTED STRANDS OF A REACTOR CONTAINMENT BY A DESTRUCTIVE TEST METHOD

REPORT 2025:1130





# Determination of stresses in grouted strands of a reactor containment by a destructive test method

PETER LUNDQVIST AND MANOUCHEHR HASSANZADEH

#### **Foreword**

This report forms the results of a project performed within the Energiforsk Nuclear Power Concrete Program. The Nuclear Concrete Program aims to increase the knowledge of aspects affecting safety, maintenance and development of concrete structures in the Nordic nuclear power plants. A part of this is to investigate possibilities to facilitate and simplify the work that is performed in the nuclear business.

In the Nordic countries, the reactor containment is designed as a cylindrical concrete structure prestressed by horizontal and vertical tendons that can be bonded or unbonded. The stress of the tendons is an important security function for the containment in case of accident.

The aim of this study is to analyze prestressed bonded tendons obtained through the decommissioning of Barsebäck nuclear power plant, to better understand the factors that influence their performance. The results show that it is possible to estimate the stress in bonded tendons through instrumentation and cutting of cables. Furthermore, the article shows that Barsebäck's tendons have lost remarkably little of their stress.

The study was carried out by Peter Lundqvist, Vattenfall and Manouchehr Hassanzadeh, Sweco. The study was performed within the Energiforsk Nuclear Concrete Program, which is financed by Vattenfall, Uniper, Fortum, TVO, Skellefteå Kraft, Karlstads Energi, the Swedish Radiation Safety Authority and SKB.

These are the results and conclusions of a project, which is part of a research Program run by Energiforsk. The author/authors are responsible for the content.



## **Summary**

Barsebäck nuclear power plant was commissioned in the early 1980s. The reactor containment structures of the nuclear power plant are built with post-tensioned bonded tendons. The nuclear power plant has been decommissioned since the early 2000s. Therefore, it has been possible to determine the stress in the tendons through destructive testing.

The tests included, among other things, the uncovering of the tendons at 9 different locations, the application of strain gauges to a large number of strands, and the cutting of the strands. Cutting of the instrumented cables allowed determination of their stress levels. In addition to measuring the stress levels of the cables, the moisture content of the outer wall of the reactor containment was also determined in order to estimate the level of drying shrinkage. This article shows that it is possible to estimate the stress in bonded tendons through instrumentation and cutting of individual strands. Furthermore, the article shows that Barsebäck's tendons have lost remarkably little of their pre-stress. This article also presents a literature review to compile similar investigations.

## **Keywords**

Tendons, Barsebäck, stress, strands



# List of content

1	Intro	duction	6
2	Meth	hods	9
	2.1	Existing methods – a literature review	9
	2.2	Tests conducted on the barsebäck NPP Reactor containment	14
		2.2.1 Structure of the Barsebäck reactor containment	14
		2.2.2 Performed tests and test locations	16
		2.2.3 Uncovering of the tendons	18
		2.2.4 Condition of the strands	20
		2.2.5 Sensors for measurements	20
	2.3	In situ RH measurements	24
	2.4	Strain measurements	24
		2.4.1 Description of the parameters and procedures	24
		2.4.2 Arrangement of the strain gauges	27
	2.5	Cutting the strands	28
	2.6	Drilling of cores for testing	29
3	Resu	lts	31
	3.1	Execution and data acquisition	31
	3.2	Results of the scans	31
4	Discu	ussion and conclusions	44
5	Refe	rences	46



#### 1 Introduction

The reactor containment (RC) enclosing the reactor vessel is the most important safety barrier in a nuclear power plant. Its main purpose is to prevent radioactive discharge to the environment in the event of a severe internal accident. In the Nordic countries, the containment is designed as a cylindrical concrete structure prestressed by both horizontal and vertical tendons. The leak tightness and structural integrity of the RC are secured by a steel liner on the inside of the RC. In Sweden, an inner conventionally reinforced concrete wall protects the steel liner from internal actions.

Typically, the corrosion protection of the tendons is accomplished either by cement grouting (bonded tendons) or by injection of, for example, grease (unbonded tendons). The main accident scenario the containment is designed to withstand is the so-called loss of coolant accident (LOCA), which can, for example, be initiated by a pipe rupture in the cooling system, causing a discharge of hot steam into the containment. The release of steam increases both the temperature and pressure inside the RC, inducing tensile stresses in the concrete walls. The tendons counterbalance these tensile forces by maintaining the concrete in a compressive state, thus securing the integrity of the steel liner.

Other functions of the RC include protecting the reactor vessel against external actions, such as aircraft crashes, explosions, and earthquakes. Due to creep and shrinkage of the concrete and relaxation of the prestressing steel, the forces in the tendons decrease over time. Since the safety of the structure depends on these forces, being able to monitor or at least estimate the prestress losses is crucial for safe operation.

For RCs with unbonded tendons, the forces in randomly selected tendons are typically measured at regular intervals during in-service inspections. However, this is not possible in RCs with bonded tendons, where no reliable means of monitoring the tendon forces are available.

The decommissioning of Barsebäck's nuclear power plant (NPP) provided a unique opportunity to investigate not only the physical and mechanical condition of the concrete but also the stresses in the grouted tendons of the outer wall of the RC. Barsebäck's NPP contains two similar boiling water reactors, which were built in the late 1970s. The NPP was decommissioned in 2005. The RCs at Barsebäck are designed as concrete cylinders with a total thickness of 1 meter, including an outer and inner concrete part (0.26 meters) and a 6 mm thick liner embedded between the outer and inner concrete parts. The RCs are 50 meters in height with an internal radius of 10.3 meters. The outer cylinder part is prestressed in both the horizontal and vertical directions. The vertical tendons are anchored near the bottom of the foundation plate and on the upper surface of the roof slab, while the horizontal tendons are anchored in four symmetrically arranged pilasters.

The foundation of the RC is a 2.4 meter thick conventionally reinforced concrete slab founded on boulder clay. The cylinder wall rests on a layer of neoprene, which is placed in a slot in the concrete foundation. The concrete used in all parts of the



RC is class I, watertight, K40 (strength class of 40 MPa based on cube tests) with Low Heat Portland Cement Limhamn. The strength classes of the conventional reinforcement were KS400S (ribbed bars, strength class 400 MPa, weldable) and KS 400, respectively. In the outer part of the cylinder wall, the conventional reinforcement was organized in a mesh consisting of Ø16 mm bars with a spacing of 300 mm.

The tendons are of the VSL type, consisting of twelve 7-wire strands with a nominal diameter of 12.5 mm. The effective steel area of each tendon is 1344 mm². In total, there are 56 vertical tendons and, on average, 3 horizontal tendons per meter of height. The tendons were initially stressed to 800 MPa (horizontal tendons, 90 kN/strand) and 1000 MPa (vertical tendons, 112 kN/strand). The ducts for the tendons were injected with cement grout consisting of low heat Portland cement, with a water/cement ratio of less than 0.4.

The RC is enclosed by a secondary concrete structure, the reactor building, which also houses auxiliary components, such as reactor pools (see Figure 1). Due to the presence of the reactor building, the RC is subjected to an indoor ambient climate with a temperature slightly higher than normal room temperature. Results from climatic measurements performed during operation in 2004 showed that both the ambient relative humidity (RH) and temperature in the reactor building vary along the height of the RC, with approximately 5-10 % RH and 50°C in the upper parts, and around 15-35 % RH and 25°C in the lower parts Nilsson and Johansson (2009). The indoor air moisture content (kg/m³) followed the outdoor variations. It was also found that the RH in the concrete close to the steel liner was between 80 % and 90 %, indicating that the concrete is still drying and most of the drying process remains.



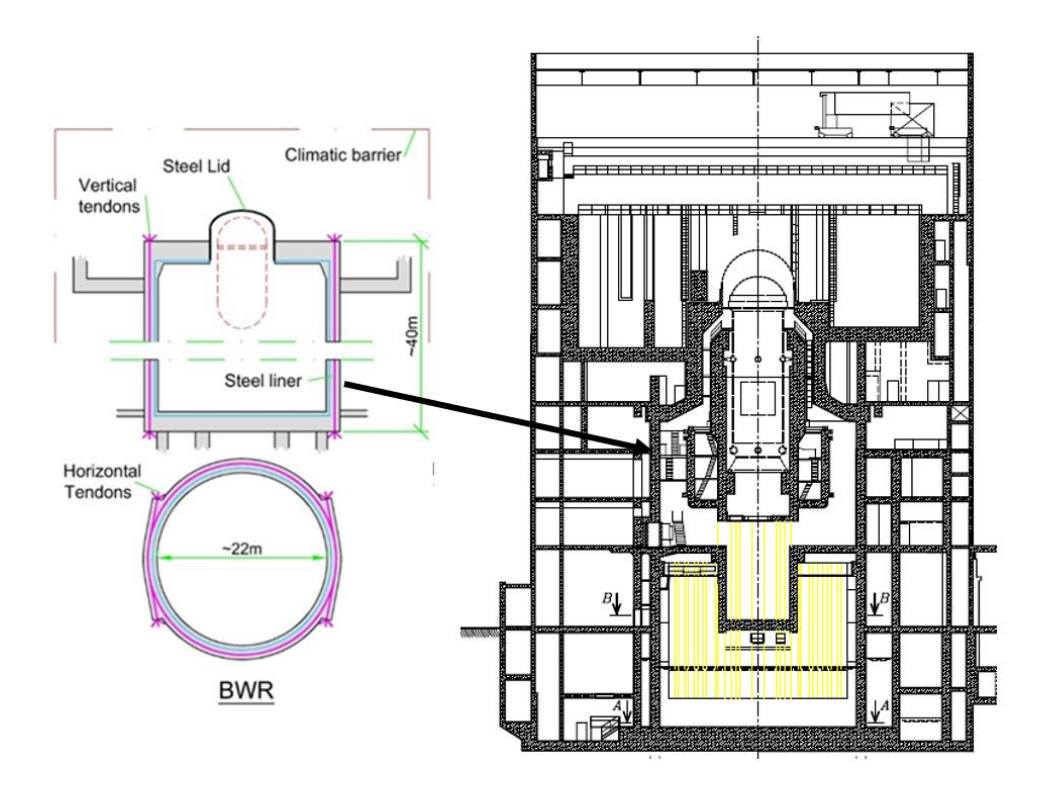


Figure 1 Right figure shows the layout of the RC and reactor building, Anderson (2006). The left figure shows the layout of the tendon system, Barslivo et. al. (2003).

A project was initiated in 2021 to investigate the status of the RCs, with a focus on the remaining forces in the grouted tendons. Considering that the tendons in the RC were tensioned and grouted approximately 50 years ago, which is a relatively long time within the context of concrete structures, it means that most potential cement reactions have taken place. Consequently, the material properties of the concrete, such as compressive strength and modulus of elasticity, have likely reached their final values. Therefore, the RCs at Barsebäck presented a unique opportunity to investigate concrete subjected to the conditions in a nuclear power plant (NPP).

The project included in-situ measurements of the forces in three of the tendons, as well as relative humidity and temperature measurements inside the concrete. Additionally, several cores were extracted from the outer cylinder wall to characterize the concrete.

This paper accounts for the part of the project that deals with uncovering, instrumenting, and cutting the strands to measure their stress levels, in-situ measurements of the concrete's relative humidity, and drilling concrete cores to fabricate specimens for determining the concrete's density, porosity, compressive strength, splitting tensile strength, and modulus of elasticity.



#### 2 Methods

#### 2.1 EXISTING METHODS – A LITERATURE REVIEW

Prestressed concrete has been used for various types of structures since the development of the method. Examples of structures where prestressing is commonly applied include bridges, floor slabs, railway sleepers, and reactor containments. Prestressing tendons are also used for anchoring concrete structures to bedrock, such as wind turbine concrete foundations and various hydropower structures.

Prestressing induces compressive stresses in the structure that counteract the main tensile stresses caused by the loads acting on the structure. In bridges and floor slabs, prestressing is intended to counteract tensile stresses caused by the self-weight of the structure, thereby reducing deflection. For RCs and railway sleepers, the main function of prestressing is to counteract tensile stresses that occur due to external loads. In RCs, the primary purpose of prestressing is to prevent cracking in the concrete under high internal pressure, such as in the event of a Loss of Coolant Accident (LOCA) when reactor cooling is lost.

Prestressed structures can be divided into two main groups: pre-tensioned structures and post-tensioned structures. In pre-tensioned structures, concrete is cast against pre-tensioned tendons. The prestressing device is disconnected from the tendons once the concrete has reached a prescribed level of strength. Since the tendon is bonded to the concrete and cannot be released, it is not possible to directly determine the level of prestressing. However, indirect methods can be used for this purpose.

In post-tensioned structures, the concrete is not cast against the tendons. The tendons are stressed after the concrete has reached a prescribed level of strength. Post-tensioned tendons are typically placed in ducts within the formwork before the concrete is cast. After the post-tensioning is completed, the ducts can be filled with cement grout, corrosion-protective grease, or left empty. When the ducts are filled with cement grout, adhesion occurs between the tendons and the ducts, which are in turn bonded to the concrete. Tendons with grouted ducts cannot be replaced or re-tensioned, and it is also not possible to directly measure the prestress force of tendons within grouted ducts. The stress of the tendons can, however, be estimated using various destructive and non-destructive test methods, which provide an estimation of the tendons' stress level.

It should be noted that there are also post-tensioned structures where the prestressing tendons are placed outside the concrete mass of the structure. For instance, the lower part of a hybrid wind turbine tower, which is made of concrete (with the upper part made of steel), may be post-stressed using tendons placed inside the tower.

Currently, there are numerous types of prestressed structures that have aged enough to necessitate an evaluation of their load-bearing capacity. However, performing a reliable evaluation requires knowledge of the prestressing force. In cases where the tendons are not bonded to concrete or grout, the prestressing force



can be assessed by applying a tensile load to the tendon until the anchor head separates from the anchor plate. In cases where the tendons are bonded to concrete or grout (known as bonded tendons), this method is not applicable, and alternative methods must be used.

Different methods used to determine the prestressing force in bonded tendons are compiled in Agredo Chávez et al. (2024). These methods are divided into non-destructive and destructive methods. Non-destructive methods can be further categorized into two groups: methods that can be applied without any intervention in the structure, and methods that require some form of intervention, even superficially, such as core drilling, sawing of the concrete, or exposing a limited length of the prestressing steel. For a detailed description of these non-destructive methods, the reader is referred to Agredo Chávez et al. (2024).

Methods that can be applied without any intervention are based on analysing the response of the structure, including deformations and strains, to loading. These methods should either be applied routinely to detect changes in structural responses or be combined with numerical models that can simulate the structure's response to the same loading. Both approaches can quantify the average changes in the tendons' stress levels. The accuracy of these methods depends on the type and number of measurement devices, the measured parameters, the type of analysis model, and the frequency of the tests, i.e., the time between the test intervals.

Methods requiring interventions, such as the hole drilling method, saw cut method, and crossbow test, are applied locally. In the first two methods, the stress release of a block of concrete on the surface of the structure is measured and translated to the stresses in the tendons. In the third method, a strand of a certain length is uncovered and loaded perpendicular to its longitudinal direction. The stiffness of the strand in the direction perpendicular to its longitudinal direction is related to the strand's stress level, allowing the calculation of the strand's stress level. None of these methods are applicable for reactor containments, particularly the crossbow test, because strands in the ducts are closely stacked and twisted around their own axis and the axis of the tendon.

Destructive methods presented in Agredo et al. (2024) are divided into two groups. In one group, the structure, usually a prestressed beam, is gradually loaded in bending until a crack is observed in the bottom of the cross-section approximately at midspan. The formation of a crack indicates that the external loading exceeds the compressive stress induced by the prestressing tendons at the location where the crack has formed. This load is called the decompression load, and the method is known as the decompression load method.

In the second method, the prestressing tendons are exposed, instrumented, and cut. By measuring the contraction strain caused by the unloading of the tendons, the prestressing force can be determined using Hooke's law.

For specific details on the different methods for estimating stresses in prestressed tendons, please refer to Agredo Chávez et al. (2024).

The decompression load can be examined and described in various ways, as outlined below:



- 1. The load recorded when the first crack is observed is assumed to be equal to the decompression load. Crack detection can be done visually or by measuring the strain of the concrete within the area where the crack is expected to first occur (Baran et al., 2005).
- 2. The structure is gradually loaded to a specified load level, and the cracks that have formed are marked. Then, the structure is unloaded, and strain gauges are installed on both sides of selected cracks. Thereafter, the structure is loaded in a quasi-static manner while strain-load curves (load presented on the horizontal axis) are recorded. The strain-load curve is initially linear, with the strain increasing as the load increases. After the load exceeds the load level corresponding to the decompression load, the strain of the concrete no longer increases. The load-strain curve changes from a linear ascending curve to a "horizontal" curve. This is because the crack is no longer subjected to compression, and the concrete on both sides of the crack becomes stress-free.

The decompression load is determined by finding the intersection point between the tangent to the ascending curve and the tangent to the horizontal curve. Usually, the procedure is repeated through unloading and reloading to determine the reproducibility of the method (Pessiki et al., 1996; Naito et al., 2008; Baran et al., 2005).

3. The same procedure as above, but with the difference that deformation gauges placed across a crack are used instead of strain gauges placed on both sides of a crack. The structure is also subjected to quasi-static loading while the load-deformation curve is recorded. The load-deformation curve is initially linear and steep, transitioning through a nonlinear ascending part to a flatter curve. The intersection points between the tangents of the steep and flatter parts indicate the decompression load (Pessiki et al., 1996; Eder et al., 2005; Baran et al., 2005).

As mentioned above, the decompression load method is used to determine the prestressing force of bonded tendons in prestressed beams. To evaluate the prestressing force, Navier's equation is used (Agredo Chávez et al., 2024). This method is applicable in a laboratory setting and is not suitable for structures in service due to the destructive nature of the test method.

The prestressing force of the tendons can also be determined through instrumentation and cutting of the tendon. This method involves exposing the tendon by removing the concrete, installing strain or deformation gauges, and then cutting the prestressing steel. During the cutting process, the tendon undergoes unloading, resulting in contraction which is recorded by the gauges. The contraction is then converted into stress using Hooke's law. Due to the destructive nature of this testing method, it cannot be applied to a structure that is in use. This method is suitable for structures that are scheduled for demolition or for structural elements that are either removed from an existing structure or manufactured in a laboratory for testing (Shenoy and Frantz, 1991; Halsey and Miller, 1996; Baran et al., 2005; Remennikov and Kaewunruen, 2015; Agredo Chávez et al., 2024).



The prestressed tendon tested in Shenoy and Frantz (1991) is a 7/16 in. (11.1 mm) strand. According to the reference, strain gauges were installed on the strands before cutting. However, the reference does not specify the number of wires in the strand, the number of strands tested, or the number of strain gauges installed. No test results are provided, and it is noted that the results were very erratic, yielding little information.

Similarly, Halsey and Miller (1996) also determined the prestressing force in pretensioned strands by installing strain gauges on the strands and subsequently cutting them. The reference does not specify the type or dimensions of the strands. However, the beams tested by Halsey and Miller (1996) are of the same type as those reported by Shenoy and Frantz (1991). The prestress loss estimated by Halsey and Miller (1996) through their tests was 34%, which was significantly greater than the losses determined by other methods used in their investigation.

Baran et al. (2005) presents tests conducted on 11 pre-tensioned I-beams. These beams were 20 ft. (6 m) in length and 28 in. (0.71 m) in height. The beams were prestressed at their lower flanges with four 0.6 in. (15.2 mm) diameter 7-wire strands, and the prestress force in the strands was 149.9 ksi (1034 MPa). During the tests, the beams were loaded in four-point bending and were instrumented with various types of deformation gauges and strain gauges. The prestress losses of the beams were determined through different methods, including instrumentation and cutting of the strands on two beams. Only the results of the strand cutting are summarized below. For other test results and theoretical analyses, refer to Baran et al. (2005).

After the tests conducted by Baran et al. (2005), two strands in each beam were exposed over a length of approximately 20 in. (0.508 m) at approximately 50 in. (1.27 m) from the end of the beam. The strands were located at the lower corners of the beams. Three strain gauges were mounted on each strand, resulting in a total of six strain gauges per beam. These gauges were bonded (glued) to each individual wire in the direction of stress.

The beams were 116 and 248 days old during the testing. The average unloading, measured as strain change, was 3710 and 3700  $\mu\epsilon$ , with a coefficient of variation of 3.6% and 4.4%, respectively. The stress in the strands was determined by applying Hooke's law, using a modulus of elasticity of 31100 ksi (214400 MPa), resulting in stresses of 115.4 and 115.1 ksi (796 and 794 MPa) for the two beams. The average prestress losses in the strands for both beams were 23%.

It should be noted that the beams were relatively young and had not been loaded previously. Baran et al. (2005) did not report any difficulties regarding the instrumentation, cutting of strands, and measurement of the strands' unloading.

Agredo Chávez et al. (2024) presents a case study involving the determination of the prestressing force of the wires in the Kalix Bridge (1956-2022), located in northern Sweden. This bridge was a prestressed concrete box-girder bridge constructed using the balanced cantilever method. The bridge was 275.7 m long with five spans and a 13-meter-wide girder deck. The box girder structure included longitudinal and transverse Dywidag bars made of high-strength steel, with a diameter of  $\varphi$  = 26 mm and grouted ducts with a diameter of 31 mm.



For the bottom slab, six bars were exposed, and one strain gauge was attached to each bar. During the cutting process, the redistribution of stresses in the parallel strain gauges was observable as the bar was being cut. The prestress data of the bars and the results of the cutting are summarized below.

For detailed information on the various testing methods, structural details, and material properties, you may refer to Agredo Chávez et al. (2024).

	Value	Unit
Measured strain after bar cutting	0.0026	
Initial prestress (as-built drawings), $\sigma_{\text{pi}}$	492	MPa
Initial prestress (prestress protocol), $\sigma_{\text{pi\_pc}}$	512	MPa
Calculated stress for the cut bar	444	MPa
Calculated force for the cut bar	245	kN
Difference between the measurements and $\sigma_{\text{pi}}$	10	%
Difference between the measurements and $\sigma_{\text{pi\_pc}}$	14	%

Agredo Chávez et al. (2024) conducted several methods to determine the reduction in prestressing stress of tendons in the Kalix Bridge. The bar cutting method showed the second lowest reduction in prestressing stress, while the Eurocode 2 method reported the highest reduction, at 27%.

In another study by Remennikov and Kaewunruen (2015), the prestressing stress in wires of 30-year-old pre-stressed railway sleepers was determined using the cutting method. The railway sleepers, used for heavy coal transportation, measured 2.5 m in length, 0.23 m in height, and 0.20 m in width. Each sleeper was pre-stressed with 24 wires arranged in 4 rows, with 6 wires per row. The wires were chevron-patterned indented wires with a diameter of approximately 5 mm.

In the study, wire cutting was performed on two sleepers from the heavy traffic railway line, and a third sleeper was selected from a railway line with mixed traffic. Strain gauges were attached to two wires in each sleeper, positioned in the top row as the second and fifth wires. During the cutting process, the strain change after relaxation was measured.

For the two sleepers from the heavy traffic railway line, the strain changes averaged 2000 microstrain. For the sleeper from the mixed traffic railway line, the strain change measured 5200 microstrain. Using Hooke's law with a modulus of elasticity of 200,000 MPa, the stress in the prestressing wires calculated to be 400 MPa and 1004 MPa, which corresponded to reductions in prestress of 60% and 23%, respectively.



# 2.2 TESTS CONDUCTED ON THE BARSEBÄCK NPP REACTOR CONTAINMENT

#### 2.2.1 Structure of the Barsebäck reactor containment

The outer cylinder part- of the RC is prestressed in both hoop and vertical directions, as illustrated in Figure 2. The vertical tendons are anchored near the bottom of the foundation slab and on the upper surface of the roof slab. The horizontal tendons stretch along approximately half the perimeter of the RC and are anchored in four symmetrically arranged vertical buttresses, as shown in Figure 3. The inner diameter of the cylinder wall gradually decreases to 6 m through a conically shaped part with varying thickness from 1.2 m to 1.0 m, as depicted in Figure 4. The liner's thickness is 5 mm in the conical part and in the upper cylinder. The upper cylinder is covered by a containment steel dome with a minimum thickness of 10 mm.

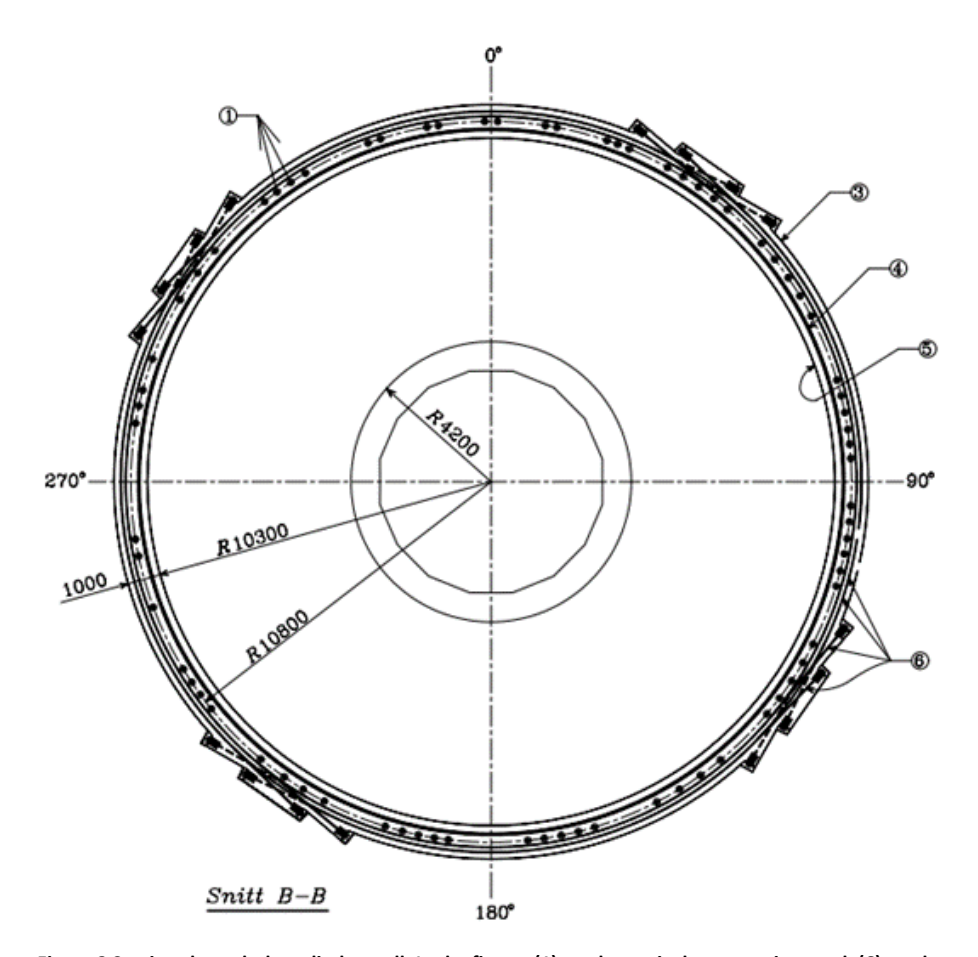


Figure 2 Section through the cylinder wall. In the figure, (1) marks vertical prestressing steel, (6) marks horizontal steel tendons anchored in four buttresses, (4) marks the liner (Roth et al., 2002).



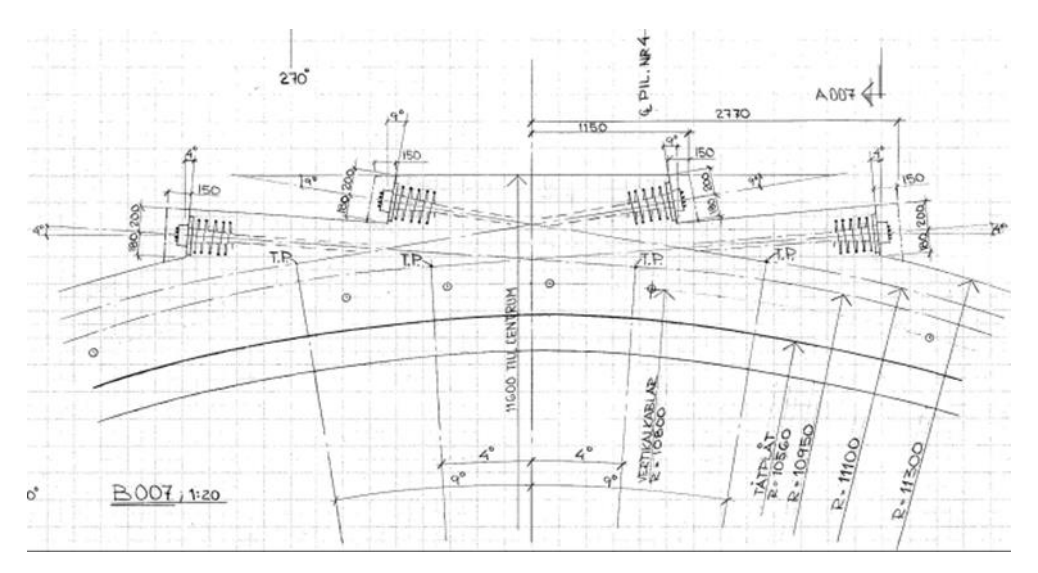


Figure 3 Position of the vertical and the horizontal tendons at a buttress.

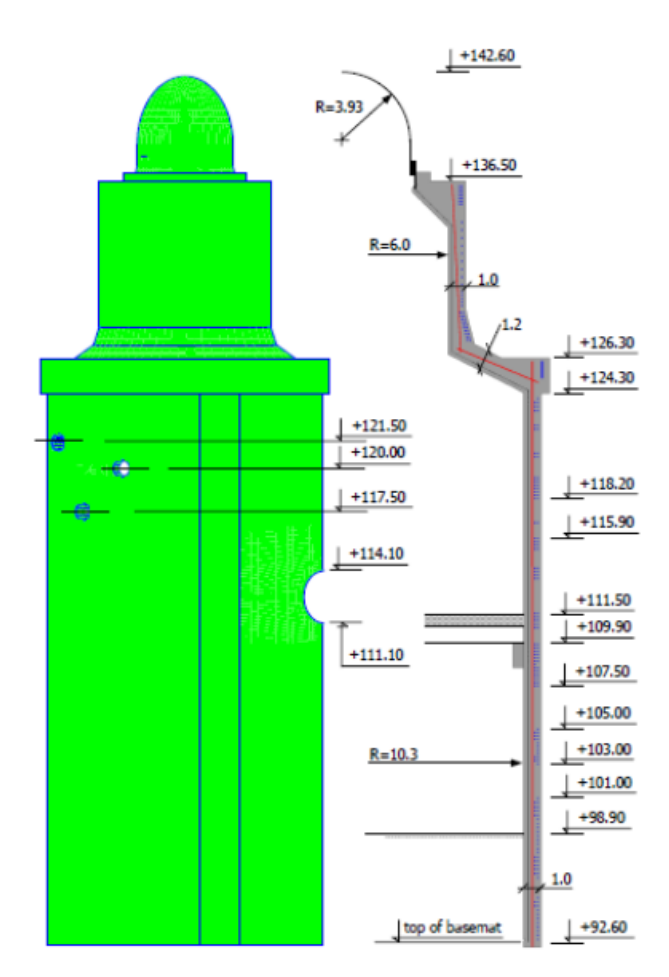


Figure 4 Main geometrical measures for the RC (Joval et al., 2002).



#### 2.2.2

#### 2.2.3 Performed tests and test locations

The test locations in the reactor building were selected based on the following prerequisites:

- availability of the working site,
- ease of installation of the working platforms,
- possibility to store the equipments and materials,
- filtering and transport of wastewater from drilling and jetting, and
- possibility to transport wastewater, concrete wastes and specimens.

The optimal location for the tests was identified to be between 157° and 215° on the horizontal plane, and between levels +101 and +113 in the vertical direction, as shown in Figure 5.

For the tests, two vertical tendons (number 39 and 41) and one horizontal tendon (number 55) were selected, as illustrated in Figure 5. The distance from the surface of the concrete to the centre of the vertical ducts, when observed from the outside of the RC, is 500 mm.

The horizontal tendons were stressed from the anchorages at the buttresses. There are 4 buttresses (1, 2, 3, and 4) positioned at 35°, 125°, 215°, and 305°, as shown in Figure 2. As depicted on the right-hand side of the drawing in Figure 5b, at some levels there are two parallel horizontal tendons; for example, the tendon-unit denoted as 55 consists of two parallel tendons/ducts. The centre of the outer duct is located 200 mm from the exterior surface of the RC, as seen in Figure 3, while the centre of the inner duct is located 350 mm from the surface. Each layer of tendon unit 55 consists of two tendons: one spans between pilasters 2 and 4 through buttress 1, and the other spans between buttress 2 and 4 through buttress 3. The tendon unit 54 consists of two layers of tendons divided into four halves, but they are anchored between buttresses 1 and 3. The outer tendon 55 was chosen as the target of this investigation.



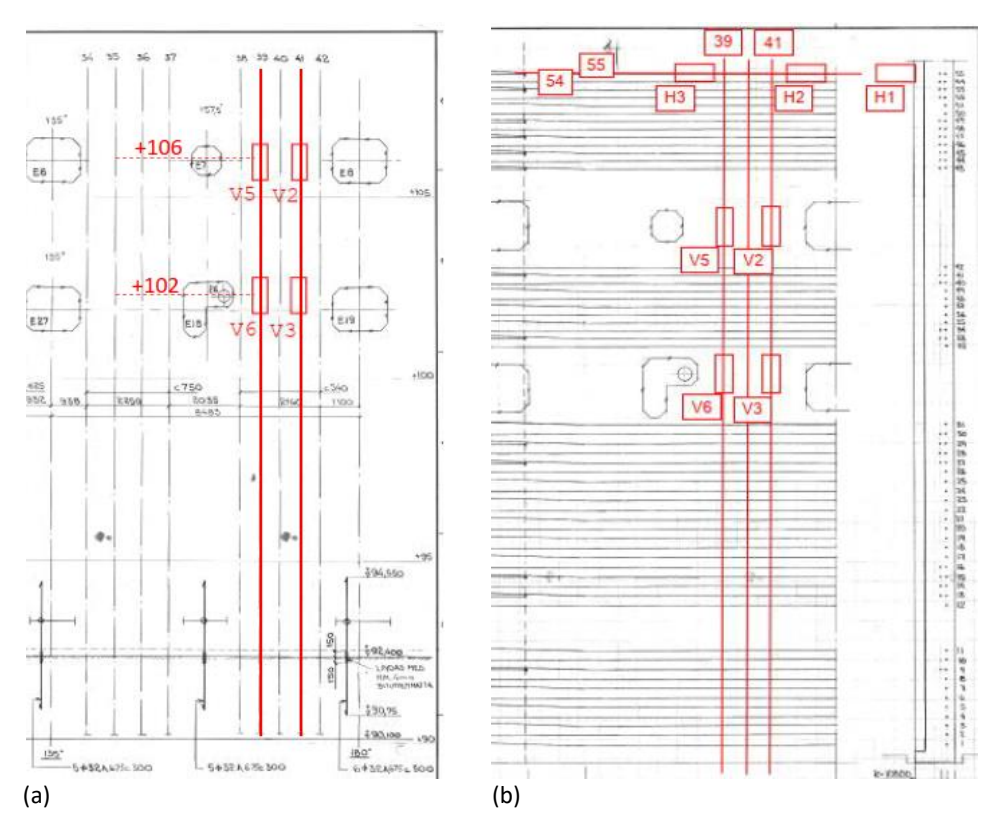


Figure 5 Location of the vertical and the horizontal tendons. (a) Vertical tendons between 130° and 180° and the levels +90 and +110. (b) Horizontal tendons between the levels +90 and +110. Please note that V1 and V4 are located just over tendon 55.

The tendons were uncovered in 9 windows, labelled V1-V6 and H1-H3, where V and H denote windows over vertical tendons and horizontal tendon respectively, as illustrated in Figure 5. Please note that V1 and V4 are located just over tendon 55. To avoid the horizontal tendons, the locations of the vertical windows were selected between RC's penetrations. The horizontal tendon-unit 55 was selected because there is an area above this unit without horizontal tendons. The space without horizontal tendons above tendon 55 facilitated the exposing of the tendon for the tests.

The dimensions of the windows were 1000 mm in the axial direction of the tendon and 500 mm in the perpendicular direction. The depth of the window was determined by the formula:  $d_{centre} + d_{duct}/2 + 100$  mm, where  $d_{centre}$  is the distance between the structure's exterior surface and the centre of the duct, and  $d_{duct}$  is the diameter of the duct (70 mm).

A ground penetrating radar (GPR) system from GSSI was used to locate the reinforcing bars and tendons. For location of the rebars, an SS mini, 1.6 GHz antenna was used. For location of the tendons, an SIR 4000 with a 1.5 GHz antenna was utilized.



#### 2.2.4 Uncovering of the tendons

A watertight shelter was erected around the windows to collect the drilling and waterjetting wastes. The reasons for this were to protect the other parts of the reactor building and to enable the transportation of the waste out of the reactor building. One shelter was constructed at each testing level. Each shelter covered either two or three windows, depending on whether the windows were over the vertical or horizontal tendons.

Wastewater from drilling and water jetting was collected in plastic IBC (Intermediate Bulk Container) units located on the floor of the reactor building. The pH of the wastewater, measured after sedimentation of the sludge, varied between 11 and 12. Radiation testing showed that the wastewater and sludge were free of radioactive substances. The water was filtered, pumped into tank trucks, and transported to a landfill site. The total volume of the wastewater was 41 m³, and the total weight of the extracted concrete waste and sludge was 6 tons.

In the first step, the exact position of the duct was identified using GPR. Concrete cores were drilled along the axial direction of the tendons to depths less than the estimated concrete cover. Then, the remaining part of the cover was removed using a hand-held waterjet lance to uncover the duct (Figure 6).

In the second step, almost all remaining concrete within the test window frame was drilled out (Figure 7).



Figure 6 Initial drilling and waterjetting to determine the exact position of the tendon



In the third step, the remaining concrete covering the duct was removed using an automated waterjetting lance (Figure 8). After removal of the concrete the duct was cut using a small circular saw blade mounted on a drill. The cutting involved two circumferential cuts spaced approximately 700 mm apart, along with an axial cut along the duct. The duct was then unrolled and removed. The grout covering the strands was removed using a hand-held waterjetting lance (Figures 9 and 10).



Figure 6 Series of drilling to remove much of concrete within the test window.





Figure 7 Uncovering the duct by means of an automated waterjetting lance



#### 2.2.5 Condition of the strands

The ability of the grout to cover the prestressing steel depends on the fluidity properties of the grout and the space available between the individual strands, as well as between the strands and the inner surface of the duct. Additionally, the arrangement of the strands among themselves plays a crucial role. The strands tend to twist around their own axis and around each other, with this twisting being more pronounced in horizontal strands than in vertical strands (see Figure 11).



Figure 9 Removal of the duct and uncovering the strands - Cut and unrolled duct



Figure 8 Removal of the duct and uncovering the strands - Waterjetted strands



Figure 10 Arrangement of horizontal strands in a duct - direction of two horizontal strands

The prestressing imposes a radial displacement on the horizontal strands, causing them to move toward the centre of the RC, thereby pressing them against the inner surface of the duct. As observed in Figure 12, the strands are stacked and forced to the left side of the duct, towards the centre of the RC. Although parts of the grout have been removed due to waterjetting and cutting of the strands, it is still evident



that the grout has not been able to penetrate the space between the strands or the space between the strands and the duct.

In vertical tendons, depending on the prestressing arrangement, the strands can be located anywhere within the duct. They might be perfectly stacked in the centre or positioned off-centre.

A visual inspection of the grout revealed that it appeared to have sufficient density and strength in areas with adequate grout thickness. However, in cases where the grout accumulated on only one side of the strands, it showed signs of cracking, possibly due to shrinkage caused by self-desiccation. In positions with insufficient grout thickness, the grout exhibited brittle and weak behaviour.



Figure 11 Grout between horizontal strands and duct

#### 2.2.6 Sensors for measurements

Three different types of sensors were used to measure three different parameters:

- 1. Relative humidity (RH) and temperature were measured by capacitive sensors (Tinytag model 4505) in drilled holes in concrete.
- 2. Temperature was measured by the sensors, TS, (PT-100) attached on the surface of the strands and concrete.
- 3. Strain was measure by resistance strain gauges, SG, glued on the surface of the wires, ducts, and concrete.

Figure 13 presents schematically the test windows, the type of the tests and localization of the sensors.



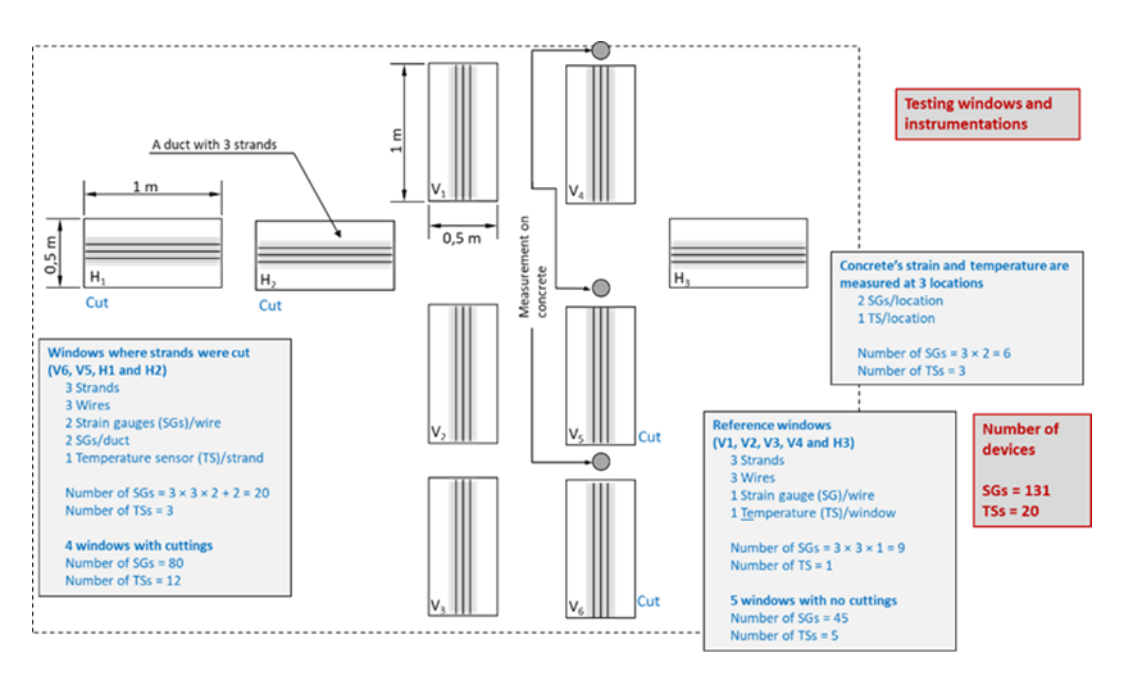


Figure 12 Schematic presentation of the test windows, type of tests and localisation of the measuring sensors

As Figure 13 shows, a total of nine test windows were included in the test program. In those windows which are denoted "Cut", all strands were cut, whereas the strands in the remaining windows, reference windows, were only instrumented with strain gauges and left uncut.

In each Cut window, 3 strands were instrumented with 6 SGs each. Three wires in every instrumented strand were instrumented with 2 SGs each. In Cut windows, the total number of SGs glued on the strands, denoted as  $SG_{cut,strand}$  was:

$$SG_{cut.strand} = 4 \text{ (windows)} \times 3 \text{(strands)} \times 3 \text{(wires)} \times 2 \text{(per wire)} = 72$$

In Cut windows, 2 SGs were also glued on the duct, i.e., one SG in the direction of the duct's axis and one in the perpendicular direction. The total number of SGs in Cut windows, denoted as  $SG_{cut,tot,\prime\prime}$  was:

$$SG_{cut,tot} = SG_{cut,strand} + 4(windows) \times 2(per\ window) = 72 + 8 = 80$$

Temperature sensors (TS), used to measure the temperature of the strand during cutting were attached to every strand equipped with SG. This resulted in a total number of 12 TS.

In each *Reference* window, 3 strands were instrumented with 3 SGs each. Three wires in every instrumented strand were equipped with 1 SG each. In *Reference* windows, the total number of SGs glued on the strands, denoted as  $SG_{ref,strand}$  was:

$$SG_{ref,strand} = 5 \text{ (windows)} \times 3(strands) \times 3(wires) \times 1(perwire) = 45$$

In *Reference* windows no ducts were equipped with SGs, and only one TS was used per window. This resulted in a total number of 5 TS.



Concrete strain and temperature were also measured at 3 locations i.e., 6 SGs (2 SGs at each location, one in the axial direction of the RC and one in the perpendicular direction), and 3 TDs.

The total number of SGs and TDs were 131 and 20, respectively.

#### 2.3 IN SITU RH MEASUREMENTS

The locations for in situ RH measurements were on level +104 (approximately 1 m over window V3), level +110,5 (between windows H2 and H3), and level +113,2 (approximately 1 m over window V4).

RH sensors were placed in drilled holes, Figure 14, with a diameter of 17 mm at depths of  $d_{drl}$ = 50, 200, 350, 500 and 650 mm. The holes were located 200 mm apart and approximately 1 m from the closest test window. The head of the sensors was placed at the depth of  $d_{drl}$ – 30 mm from the surface. An electric (plastic) pipe with an inner diameter of 16 mm was inserted inside the holes, where the RH sensors were installed. The length of the pipes was  $d_{drl}$ – 30 mm. Hence, the sensor measured the average RH of a 30 mm long segment in front of the sensors.

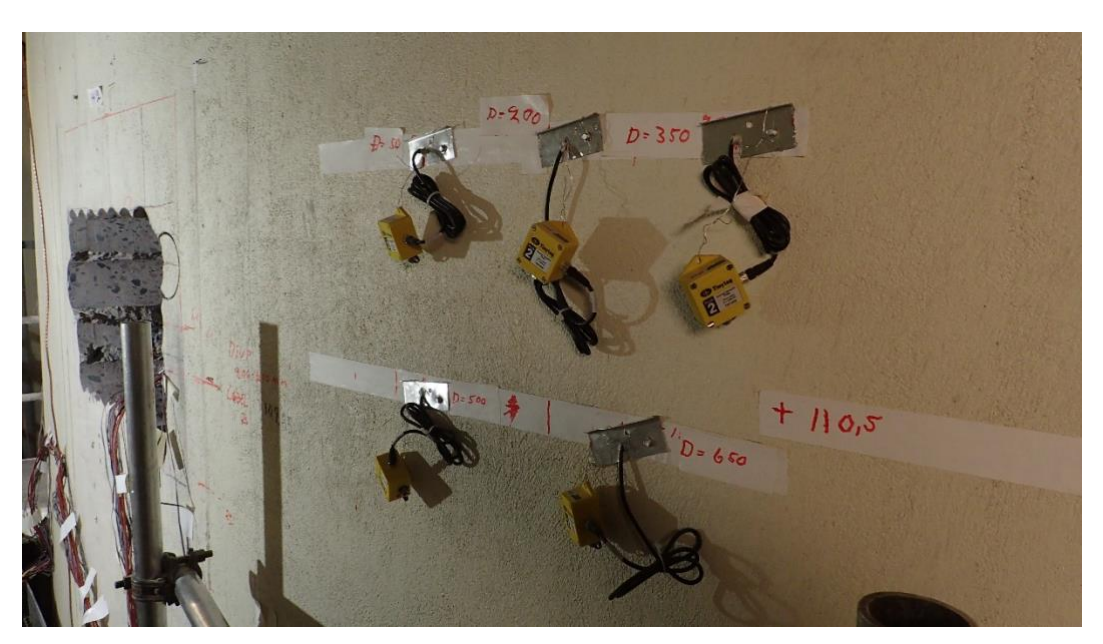


Figure 13 Installation of moisture measuring sensors on level 10,5.

#### 2.4 STRAIN MEASUREMENTS

#### 2.4.1 Description of the parameters and procedures

Strain measurements were conducted using SGs glued to individual wires. Note that the SGs were glued in the axial direction of the wires and not in the axial direction of the strands. This procedure was used because the force is transmitted in the axial direction of the wires. When the strain is measured in one direction and within a limited length, it is more accurate to position the SG in the direction of the



force. Below, the method by which the unloading of the strands was measured is presented.

Figure 15 shows the results of strain measurements during the cutting of strands in test window H1. Figure 16 schematically shows the strains of three wires before, during, and after cutting. As can be seen, different SGs show different values at time t = 0. This is due to the strains that are imposed on the SGs during and after the gluing process. Additionally, the value of SG is affected by the variation of strains in wires caused by changes in tension and temperature after the glue has hardened.

 $\varepsilon_{i,b}$  and  $\varepsilon_{i,a}$  are the strains (m/m) of the individual wires just before and after the cutting. The difference between these strains is  $\Delta\varepsilon_i$ . Each individual wire is numbered with "i" = 1:n. The purpose of the instrumentation is to determine the unloading of the strand after cutting. The unloading of the strand is assumed to be proportional to the mean value of the unloading of the individual wires:

$$\Delta \varepsilon_{str} = k_c \cdot \frac{1}{n} \cdot \sum_{1}^{n} (\varepsilon_{i,b} - \varepsilon_{i,a}) = k_c \cdot \frac{1}{n} \cdot \sum_{1}^{n} \Delta \varepsilon_i$$

where

 $\Delta \varepsilon_{str}$  = unloading of strand (m/m)

n = number of wires with SG

 $k_c$  = coefficient of proportionality

Other parameters are defined in Figure 16 and 17.

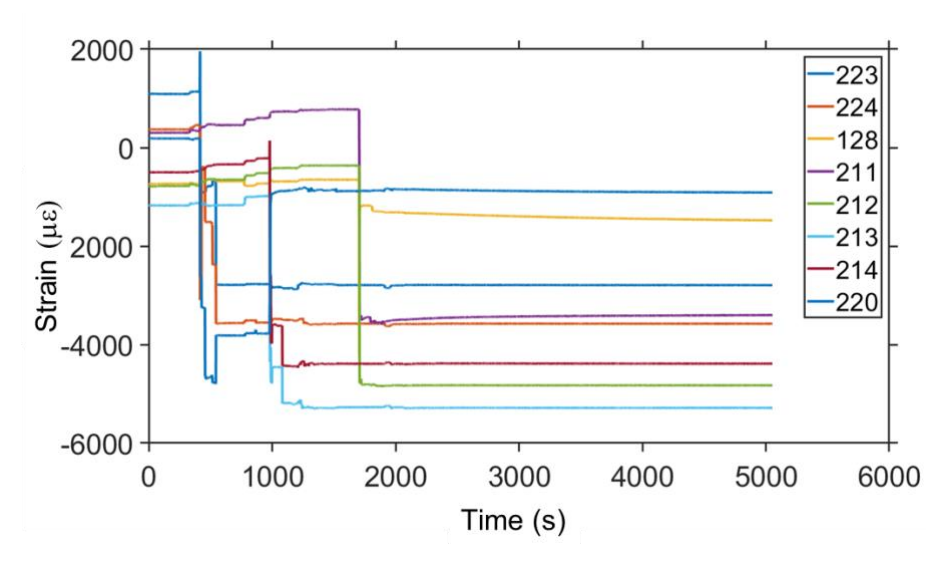
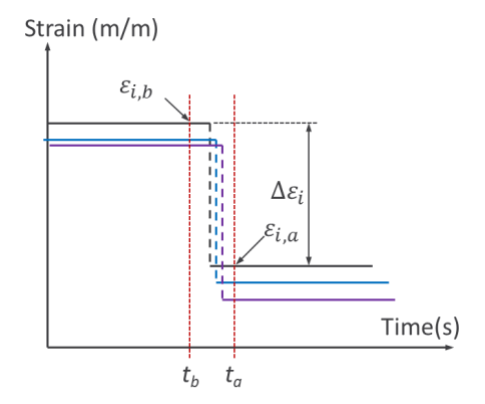


Figure 14 Results of strain measurements during cutting of strands in test window H1





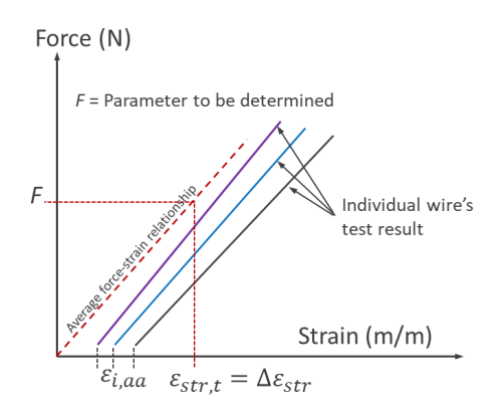


Figure 16 Schematic presentation of strain-time relation measured during the cutting

Figure 15 Schematic presentation of force-time relation which is measured by a testing machine at a laboratory

After the test performed at the site, the cut strands were reassembled and tested in a laboratory using a testing machine. The strain of a wire just before reassembling is denoted as  $\varepsilon$ \_(i,ba). When the strand is assembled in the testing machine, the strain may change to  $\varepsilon$ \_{i,aa}. Preferably, all three strain values after cutting will be equal.

$$\varepsilon_{i,a} = \varepsilon_{i,ba} = \varepsilon_{i,aa}$$

but it is more likely that they will differ from each other.

$$\varepsilon_{i,a} \neq \varepsilon_{i,ba} \neq \varepsilon_{i,aa}$$

If the difference between  $\varepsilon_{i,a}$  and  $\varepsilon_{i,ba}$  cannot be explained by temperature changes (the changes must be of the same order of magnitude as temperature effects), the effects of other influencing factors should be investigated, such as sensor operation or changes in the shape of the cut strand, etc.

Figure 17 shows a schematic presentation of the test results obtained from a tension test carried out in a testing machine. As can be observed, the strain in the wires may change when they are clamped in the testing machine, i.e., the wires obtain an initial strain. It should be noted that the initial values can be positive or negative. If the SG of the wire is not damaged during the cutting process, the load-strain curve of the wire will be linear. The load in the diagram refers to the load carried by the strand and does not pertain to the load carried by the individual wires.

The individual curves in Figure 17 is reset, and the mean value of the reset (zeroed) curves is determined. Following relationship between strand's strain in the testing machine,  $\varepsilon_{str,t}$ , and the wires' reset strains in testing machine,  $\varepsilon_{i,t}$  exists:

$$\varepsilon_{str,t} = k_t \cdot \frac{1}{n} \cdot \sum_{1}^{n} \Delta \varepsilon_{i,t}$$



where,

 $k_t$  = coefficient of proportionality

 $k_c = k_t$ , then the load of the strand before cutting, F, is determined by means of the relationship presented in Figure 17.

#### 2.4.2 Arrangement of the strain gauges

Figure 18 shows positions of the SGs on the strand. The length of testing windows is approximately 1 m. The strands are cut at approximately 0.15 m from its ends, leaving a length of 0.7 m for testing.

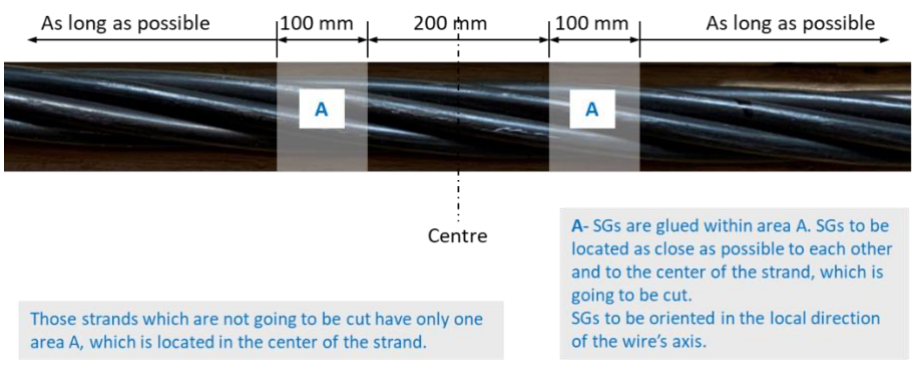


Figure 17 Positions of the strain gauges on a strand

As was mentioned previously, the strands are twisted around their own axis and also around axis of the tendon, which often made it difficult to comply with the arrangement in Figure 18. Furthermore, attempts were made to trace the same strand in different testing windows within the same tendon. This was done in order to attach SGs on the same strand to monitor the strand's response in different testing windows when it was being cut. Unfortunately, it proved difficult to identify the target strand in different windows. Figure 19 shows strain gauges and temperature sensors attached to strands in the test window H1.



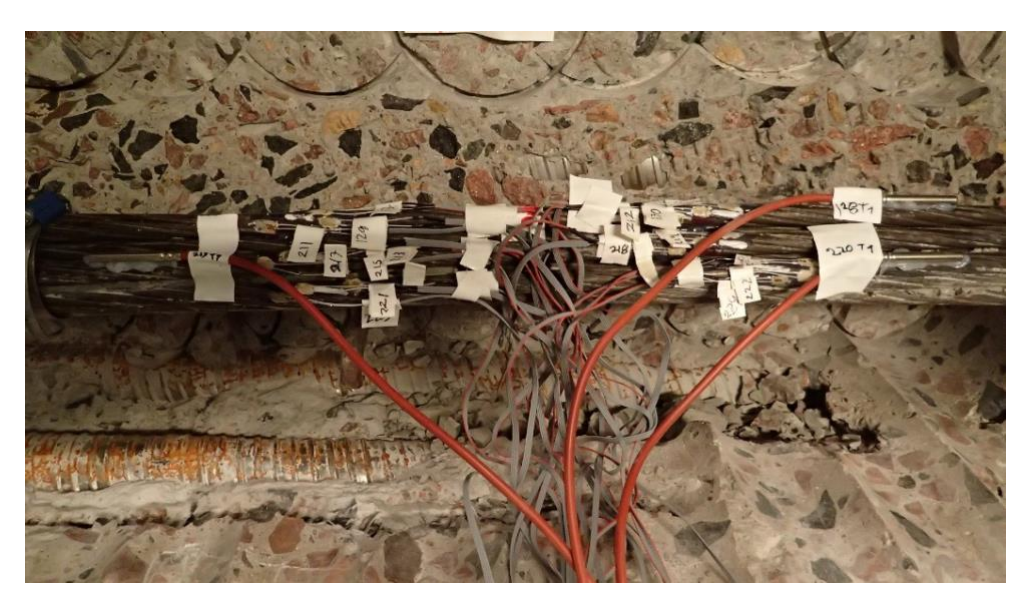


Figure 18 Strain gauges and temperature sensors attached to the strands in test window H1 (strands were cut).

#### 2.5 CUTTING THE STRANDS

The strands were cut by means of an angle grinder, as shown in Figures 20 and 21, following the planned cutting scheme:

- 1. Cut 2 strands without SGs followed by 1 strand with SGs.
- 2. Repeat the steps in point 1 two additional times.
- 3. Cut the remaining 3 strands without SGs.

Due to the close stacking and twisting of strands, it was not possible to follow the scheme in all cases. However, in all instances, two strands without SGs were cut first before any strand with SGs was cut.



Figure 19 Cutting off the strands by means of a grinder



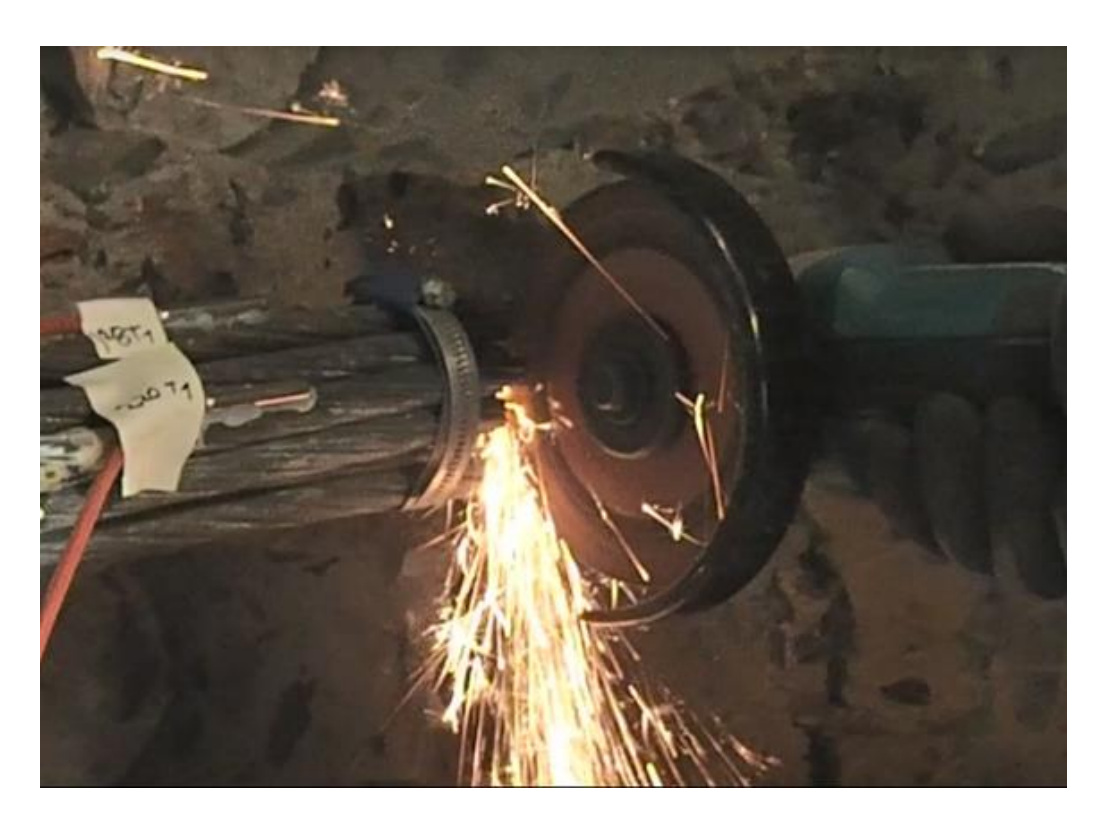


Figure 20 Cutting off the strands by means of an angle grinder.

#### 2.6 DRILLING OF CORES FOR TESTING

Specimens for determining various properties of the concrete were drilled out during the preparation of the test windows. The cores were drilled in a manner that allowed them to be used for preparing concrete test specimens. Error!

Reference source not found. presents the type of tests, the number of specimens, and their sizes used for determining different properties of the concrete. The cores were drilled as follows:

Series A: drilled at windows V1 and V4,

Series B: drilled at windows V2 and V5,

Cores for shrinkage and creep tests: drilled at windows V3 and V6.

Test	Number of specimens	Specimen size
Density and porosity	8 (divided in series A & B)	Ø100 mm, L100 mm
Compressive strength	8 (divided in series A & B)	Ø100 mm, L200 mm
Splitting tensile strength	8 (divided in series A & B)	Ø100 mm, L200 mm
Modulus of elasticity	8 (divided in series A & B)	Ø100 mm, L200 mm
Shrinkage	5	Ø100 mm, L400 mm
Creep	12	Ø100 mm, L400 mm

Table 1 Type of tests, number, and size of specimens.



Three specimens were prepared for shrinkage testing immediately after drilling. They were weighed, equipped with studs, and weighed again. Three pairs of studs were glued onto the drilled cores, with an angular distance of 120° between each pair. The distance between the studs was measured using a reference rod equipped with a measuring clock. The specimens were then wrapped in several layers of blown film and thick plastic foils and sent, along with the reference rod, to the testing laboratory. Shrinkage measurements are still ongoing in the laboratory.

All other drilled cores were wrapped in several layers of thick plastic foils, placed in strong wooden boxes, and dispatched to the laboratory for further testing.



#### 3 Results

#### 3.1 EXECUTION AND DATA ACQUISITION

Cutting of the strands was carried out in the order presented in Table 2.

Due to the limited capacity of the data acquisition equipment – only 32 sensors could be scanned simultaneously – it was not possible to scan all strain sensors on the wires and store their measurements during the cuts. Therefore, all sensors were scanned before each cut. The designations of the scans, which are also used in the figures, are shown in Table 2.

	Name of scanning	Window where the strands are cut
1	Initial scanning	
		V6
2	V6 is cut	
		V5
3	V5 is cut	
		H1
4	H1 is cut	
		H2
5	H2 is cut	

Table 2 Order of scanning of gauges and windows where the strands were cut

#### 3.2 RESULTS OF THE SCANS

The results of scans from sensors at windows V2, V4, and H3 are presented in Figure 22 - Figure 24. No strands were cut in these windows. The results show the reactions of different strands when strands in other windows were cut. The strands in windows H3 and V4 respectively were placed in the same duct as the strands in windows H1 and H2; and V5 and V6 that were cut. It should be noted that all strands in windows H1, H2, V5, and V6 were cut. No strands in the duct containing strands from window V2 were cut.

Figure 22 shows the results of scanning strain gauges on three strands (SI, SII, and SIII) in window V2. The strain gauges were glued onto three wires in each strand, one gauge per wire. As shown in Figure 22, most of the wires in window V2 exhibit some degree of unloading when the strands in window V6 are cut. The wires do not react when the strands in window V5 are cut. However, the wires react when the strands in window H1 are cut. Some of the wires that had been unloaded are loaded again, and some that had received less loading are unloaded again. The wires do not react when the strands in window H2 are cut. However, it is difficult to explain the behaviour of the wires without some numerical modelling. It is probably the redistribution of stresses in the concrete that affects the stresses around the duct that contains the strands of window V2.

Figure 23 shows the results of a similar scan as the one above, conducted on the strands in window V4. The strands in window V4 are located in the same duct as



the strands in windows V5 and V6. The intention was to identify three strands running through windows V4-V6 and preferably identify three wires in each strand in all windows. However, the task proved to be too difficult to carry out, so it was omitted. The strands and wires in each window were selected solely based on the ease of attaching the strain gauge to the strand.

As shown in Figure 23, the strands in window V4 did not react to the cutting of the strands in windows V6 and V5, despite the fact that all strands in both windows V6 and V5 were cut. The results show that the combined effect of adhesion between the strands and the injection grout, and the friction between the strands is sufficiently large for the strands to achieve full anchorage within the distance between windows V5 and V4. Almost all wires within window V4 react to the cutting of strands in window H1 but not to the cutting of strands in window H2, despite the fact that window H2 is closer to V4 than H1.

Figure 24 shows the results of the scan conducted on the strands in window H3. The strands in window H3 are in the same duct as the strands in windows H1 and H2. As shown in Figure 24, the strands in window H3 are relieved when the strands in window V6 are cut, but they do not react when the strands in window V5 are cut. The strands in H3 are loaded again when the strands in window H1 are cut but do not react when the strands in window H2 are cut.

Figure 25 and Figure 26 show the strains in some strands in window V5 and V4 while the strands in window V6 are being cut. As shown in the figures, the observed strands do not react to the cutting of strands in window V6. The same behaviour was noted in the strands in window V4 and H3 during the cutting of strands in window V5, as well as in the strands in window H3 during the cutting of lines in window H1 and H2.

According to the above results, the combined effect of the adhesion of the strands to the injected grout and the friction between the strands is sufficient for the strands to achieve a high tension level after cutting. The results also show that cutting the strands leads to stress redistribution in the concrete, affecting the tension force of the strands. Assuming the steel's modulus of elasticity is 195 GPa, 1000 microstrain corresponds to 195 MPa stress in the steel and 22 kN force in each strand. In some strands, the strain change exceeds 1000 microstrain.



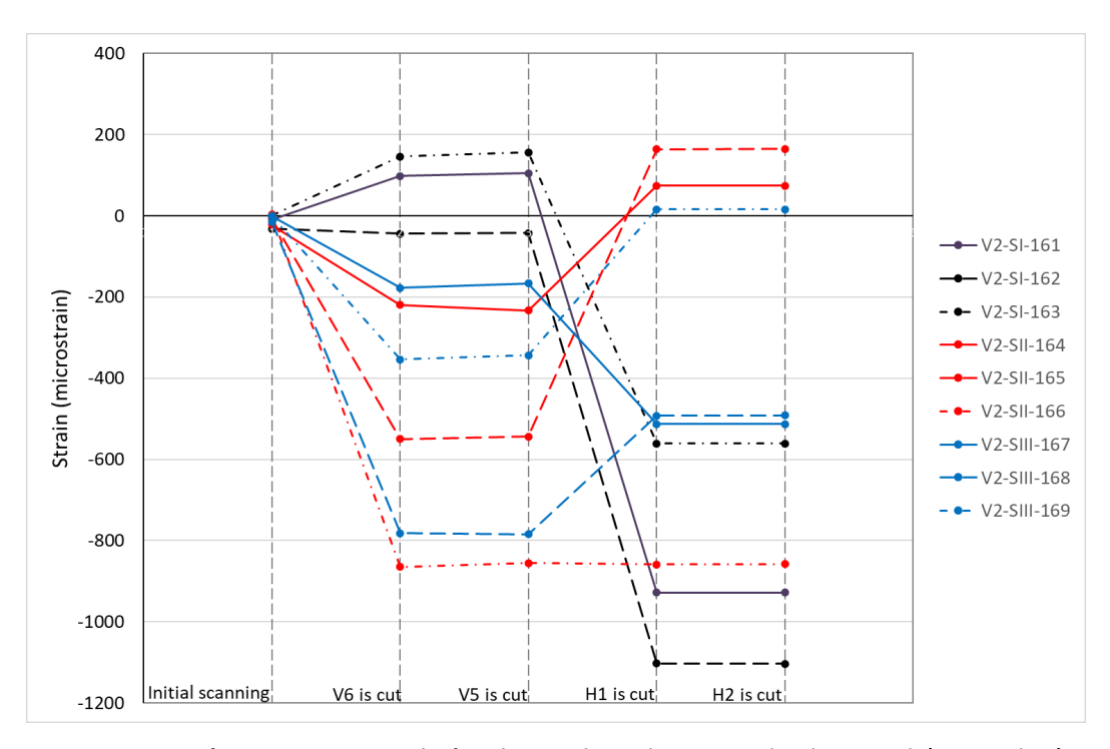


Figure 21 Scanning of strain gauges on strands of window V2. The results correspond to three strands (SI, SII, and SIII) in window V2. Strain gauges were glued to the three wires, with one gauge per wire, in each strand

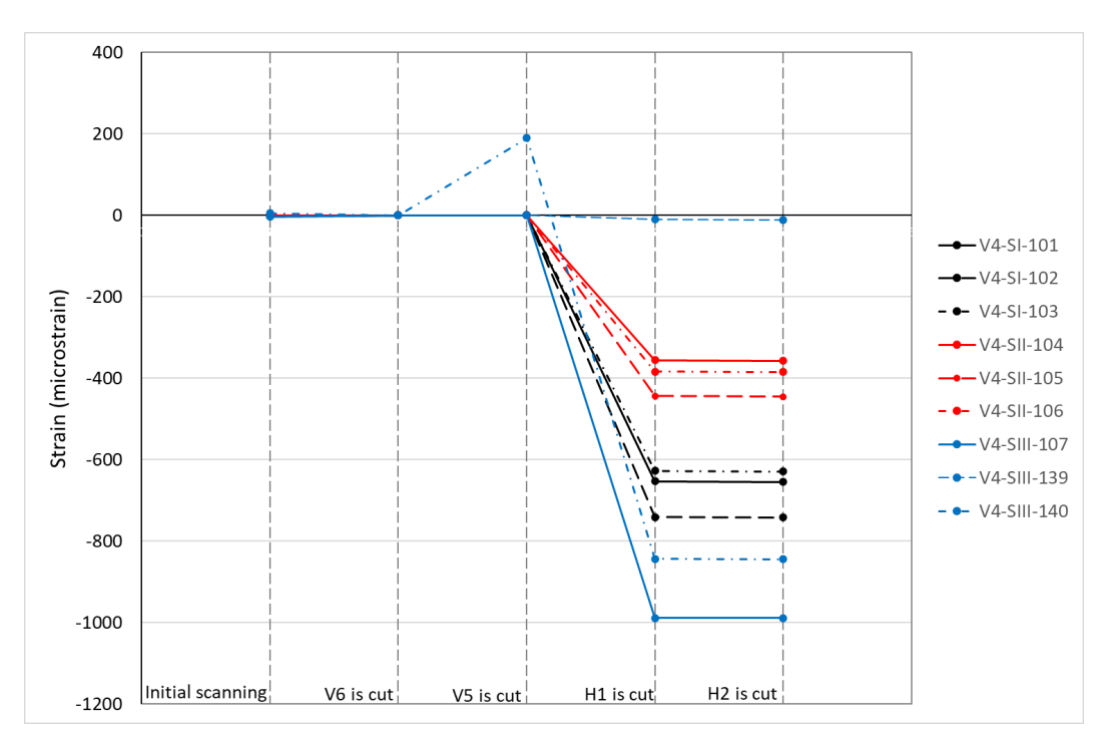


Figure 22 Scanning of strain gauges on strands of window V4. The results correspond to three strands (SI, SII, and SIII) in window V4. Strain gauges were glued to the three wires, with one gauge per wire, in each strand



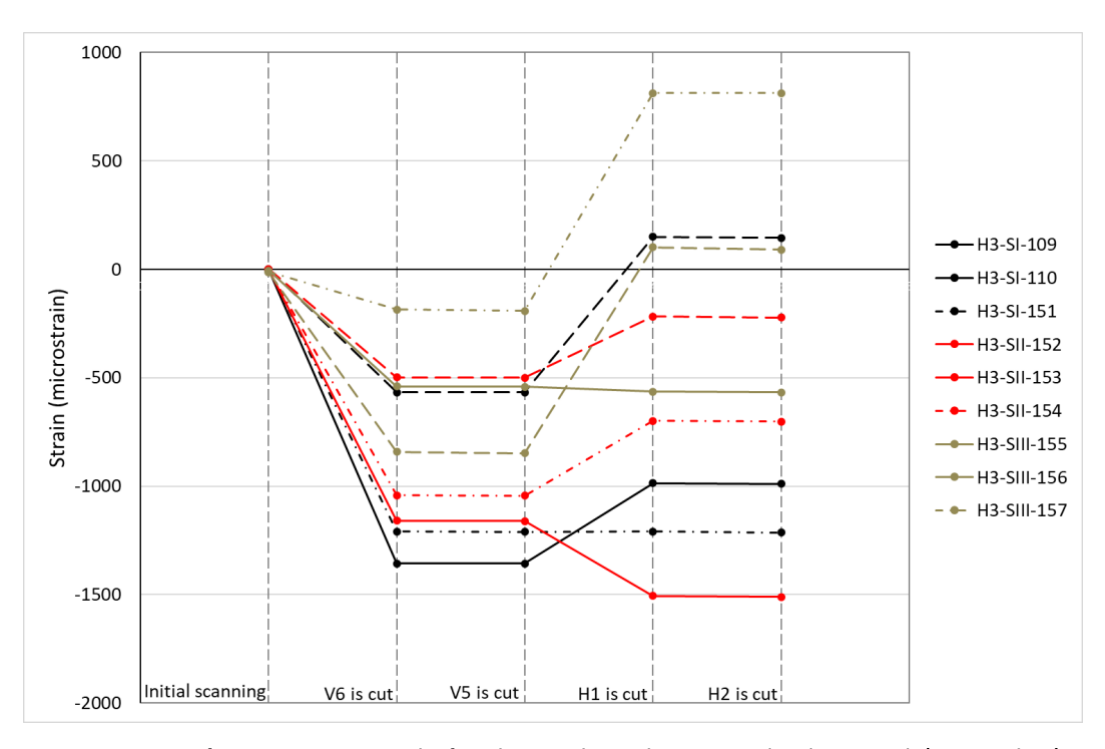


Figure 23 Scanning of strain gauges on strands of window H3. The results correspond to three strands (SI, SII, and SIII) in window H3. Strain gauges were glued to the three wires, with one gauge per wire, in each strand

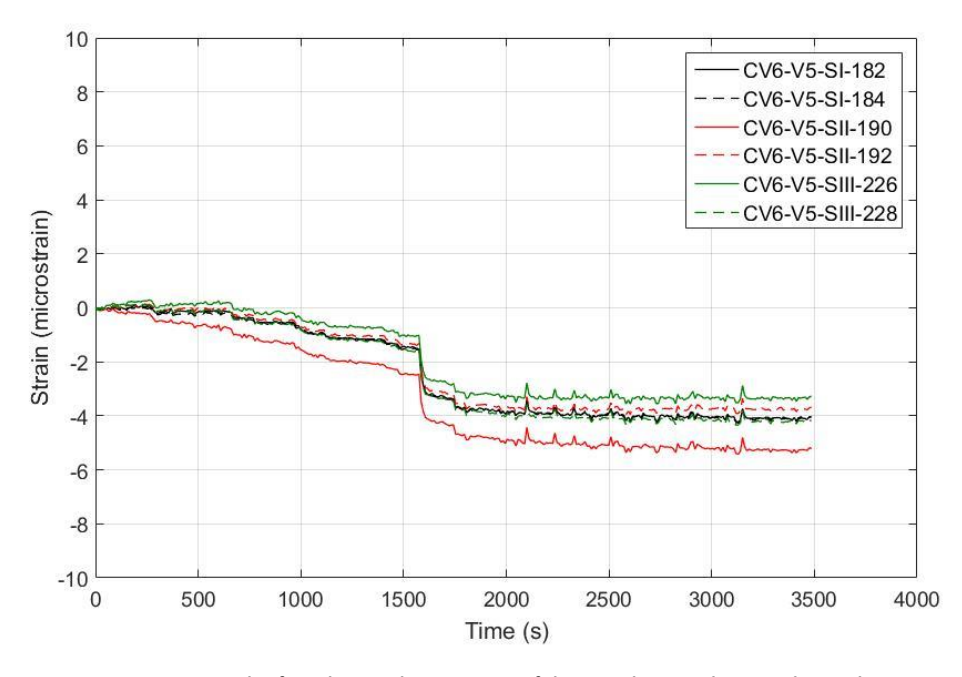


Figure 24 Strain gauges on strands of window V5 during cutting of the strands in window V6. The results correspond to three strands (SI, SII, and SIII) in window V5



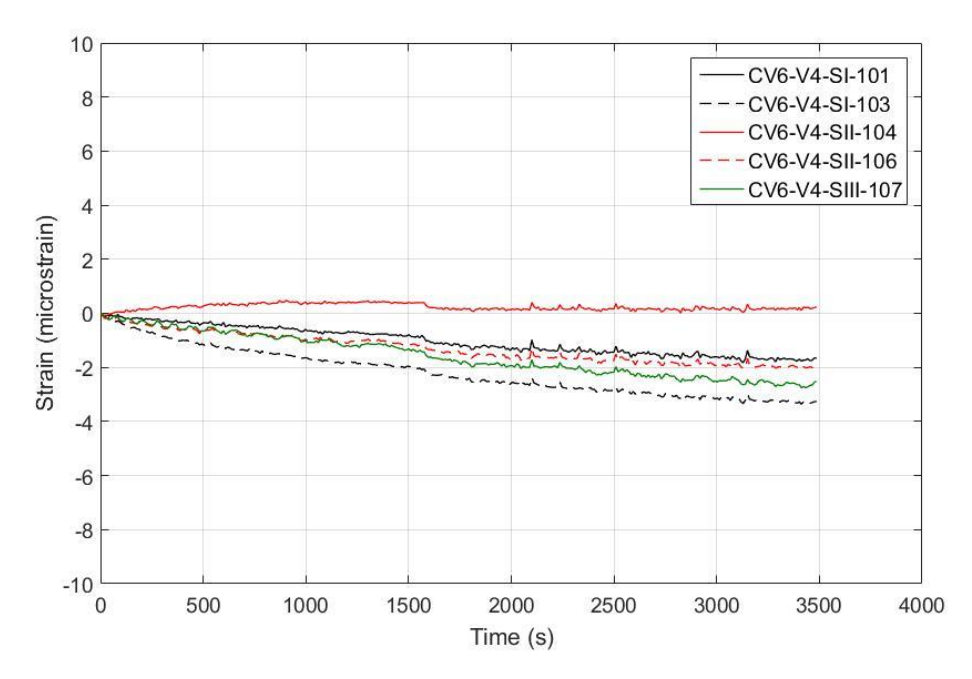


Figure 25 Strain gauges on strands of window V4. The results correspond to three strands (SI, SII, and SIII) in window V4

Figure 27 shows the results of the measurement of concrete strain over windows V4, V5, and V6. The strains are measured both in the vertical (V) and horizontal (H) directions. Due to limited scanning capacity, the measurement results are not sufficient to draw definitive conclusions. However, the results indicate relatively large stress redistributions associated with the cutting of tendons. According to the results, the concrete is subjected to large tensile strains, which can be explained by the tendons contracting during the cutting, thus unloading the concrete. The measured tensile strains in concrete must be added (by sign) to the compressive strains which were imposed during the prestressing in order to determine the prevailing state of strain of the concrete, which has not been done in this work.



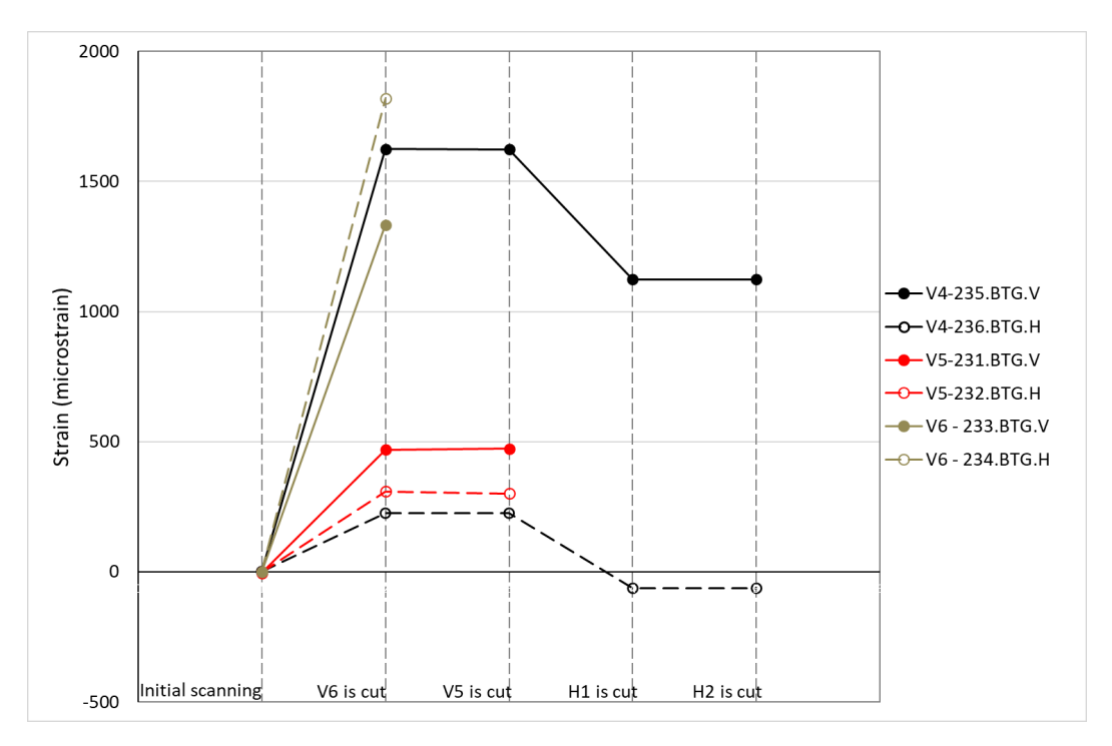


Figure 26 Results of strain gauges attached on the concrete over the windows V4, V5 and V6. Strain gauges marked with V and H correspond to vertical and horizontal directions respectively

Figure 28 shows the results of the measurement of the duct's strain in windows H1, H2, V5, and V6. The measurements have been carried out both in the longitudinal direction (L) and the hoop direction (H) of the duct. The placement of the strain gauges is shown in Figures 29 and 30. Here too, the measurement data are not sufficient to draw definitive conclusions. However, the results still indicate that the duct is subjected to relatively large strains caused by stress redistributions in the concrete and the strands. The duct contracts in the longitudinal direction when the strands in window V6 are cut. The ducts in windows H1 and H2 are subjected to tensile strains in the longitudinal direction when the strands in window H1 are cut.



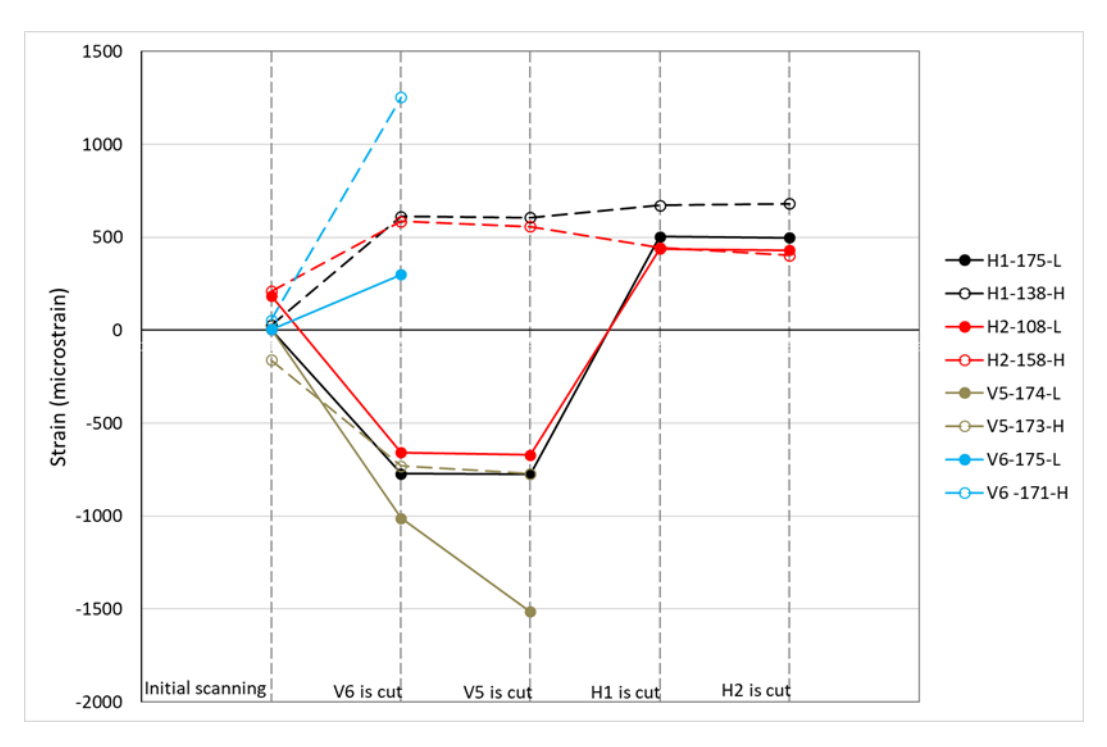


Figure 27 Results of the strain gauges attached on the ducts. Strain gauges marked with L and H correspond to longitudinal and hoop directions of the duct respectively



Figure 28 Attachment of strain gauges on the duct, window V5 before and after cutting of the strands



Figure 29 Attachment of strain gauges on the duct, window V5 before and after cutting of the strands



Figure 31 and Figure 32 show strain changes in some wires during the cutting of strands in windows V5 and H1. Three wires in three different strands (SI, SII, and SIII) were equipped with two strain gauges each, i.e., a total of six strain gauges per strand. The figures show three distinct instances when the equipped tendons are cut. It should be noted that some wires did not behave as expected and did not show the anticipated unloading. The reason for this could not be determined. It may be due to the strain gauges being damaged when the tendons twisted during the cutting. As shown in the figures, the vertical wires exhibit approximately 5000 microstrain contraction. The corresponding value for the horizontal wires is 4000 microstrain. The same tendencies were noted in windows V6 and H2.

Assuming that the tendons' modulus of elasticity and effective area are 195 GPa and 1344 mm² respectively, the stresses and forces in the vertical and horizontal tendons can be estimated at 975 MPa and 1310 kN respectively, and 780 MPa and 1048 kN respectively. The forces corresponding to the vertical and horizontal strands are 109 kN and 87 kN respectively.

Figure 33 shows temperature changes in some wires in window H1 during the cutting process. It should be noted that the temperature sensors were placed close to the cutting locations, which were far from the strain gauges.

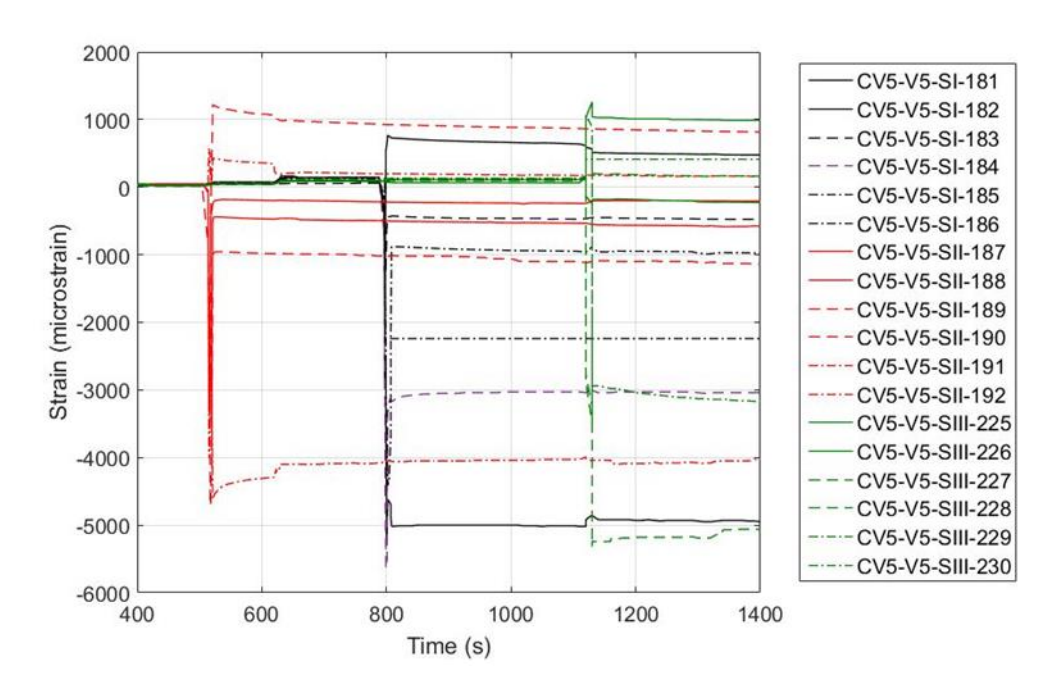


Figure 30 Strains in the wires were measured during the cutting of the strands in window V5. Three wires from three different strands (SI, SII, and SIII) were each equipped with two strain gauges, resulting in a total of six strain gauges per strand



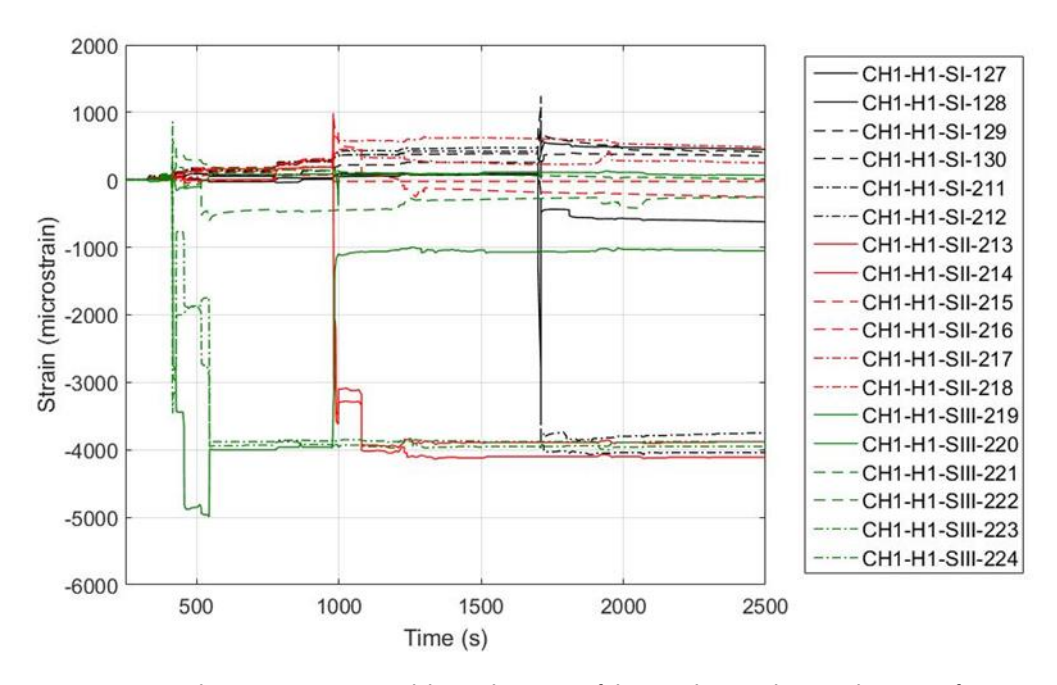


Figure 31 Strains in the wires were measured during the cutting of the strands in window H1. Three wires from three different strands (SI, SII, and SIII) were each equipped with two strain gauges, resulting in a total of six strain gauges per strand

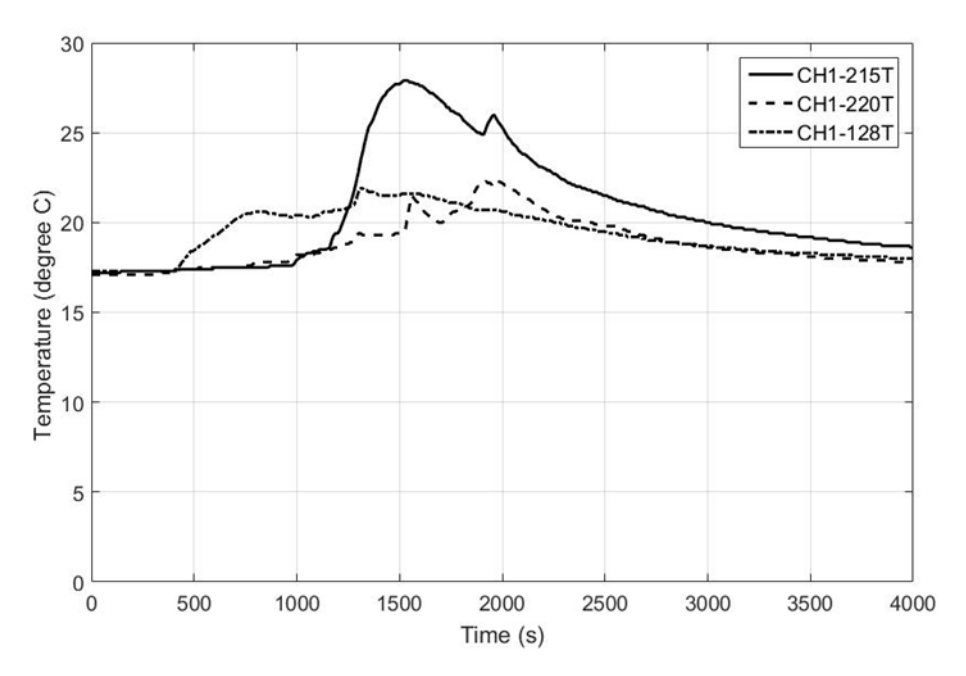


Figure 32 The temperature changes on three wires in window H1 were monitored during the cutting of the corresponding strands

Figure 34 and Figure 35 show the results of tensile tests performed with strands taken from windows V5 and V6. During the cutting and transport of the strands, many strain gauges were damaged. The two strands whose results are presented



below have worked well. As shown in the figures, the strands were pulled to a load level that was slightly above their pre-tensioning level. As mentioned in section 2.4.1, the aim was to load the tendons until the wires achieved a strain level they had at the time of cutting, but the method did not work as intended. However, plateaus were noted, see horizontal lines at the levels 113 and 134 in Figure 34 and Figure 35. The plateaus were assumed to be the load level at which all the wires reached their original strain levels at the time of cutting. As shown by the load-strain curves, the curves rise sharply after the plateaus. The strand's stiffness could have been determined if the loading had continued, but that possibility did not exist in the laboratory. The strand's stiffness could be used along with Hooke's law to determine the tendon's tension force at the time of cutting. The strands' tension force is the distance between the lower horizontal line and the upper horizontal line. The strands' tension force are 105 kN for window V5 and 131 kN for window V6 - with an average value of 118 kN which corresponds well with the tension force of 109 kN which was estimated earlier in the report using Hooke's law and the average strain.

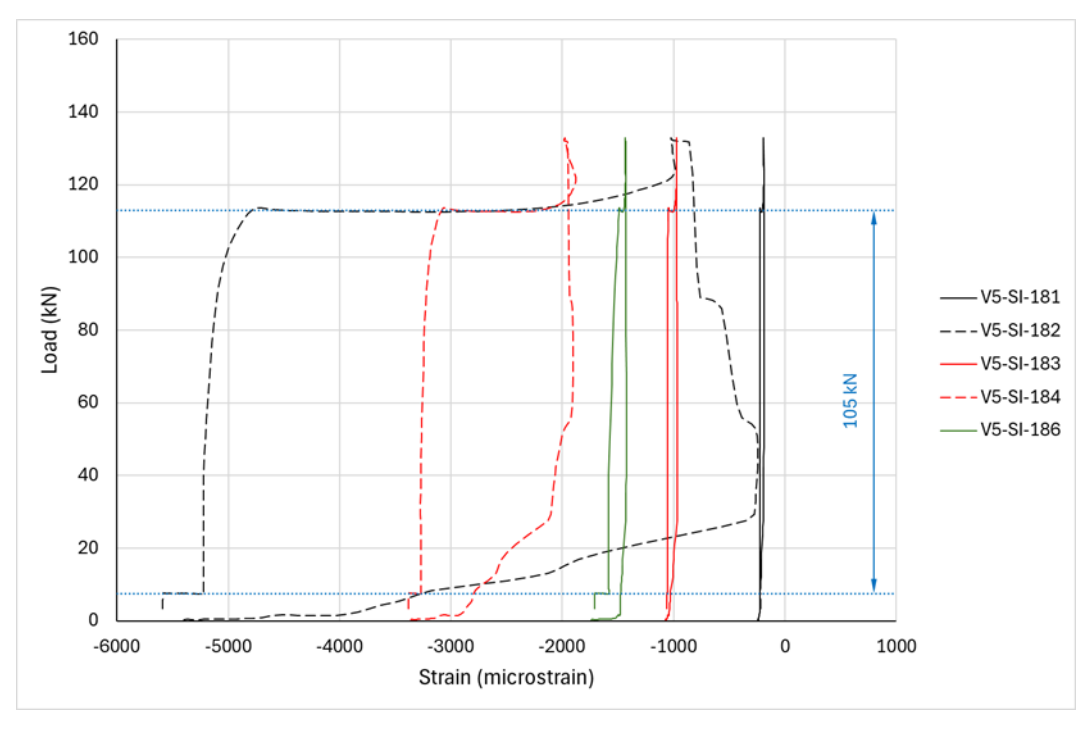


Figure 33 Result of the tensile test on a strand cut from the window V5.



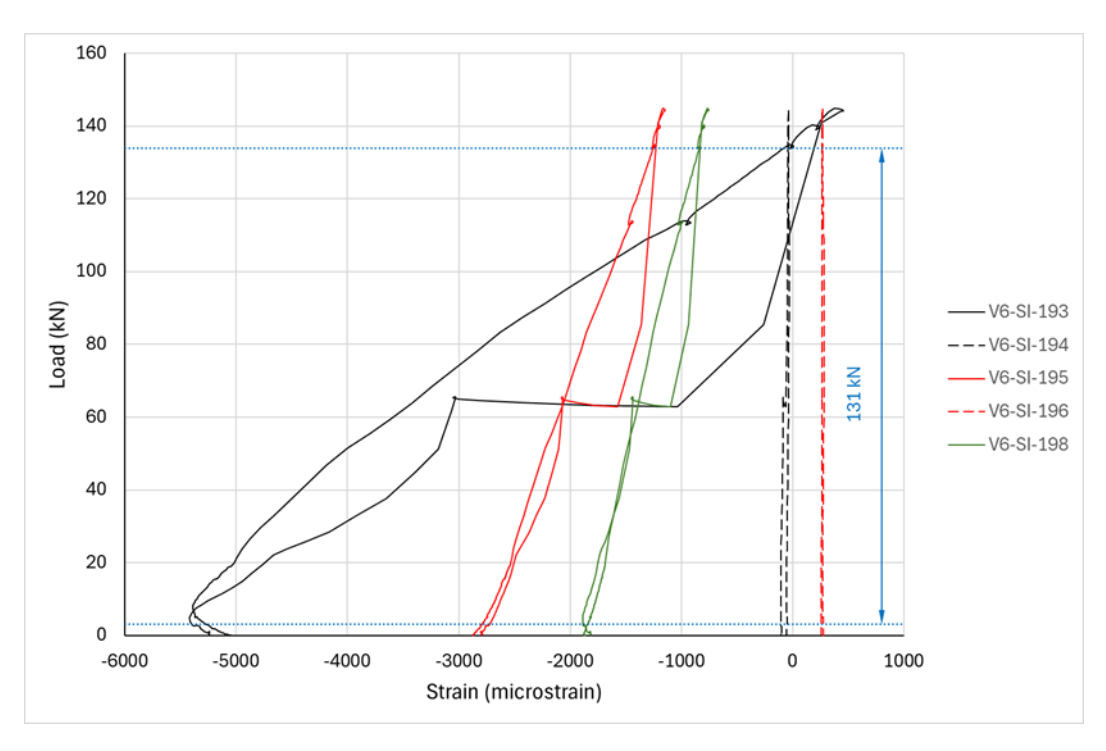


Figure 34 Result of the tensile test on a strand cut from the window V6

Figure 36 - Figure 38 show the results of RH measurements at different levels on the outside of the reactor containment. The measurements show equilibrium RH at different depths in the outer wall of the reactor containment. The measurement sensors were placed in the holes for about a month so that the moisture level of the holes and the sensors could stabilize and reach an equilibrium state, which unfortunately was not achieved in some holes. The results generally show that concrete placed deeper than 500 mm is very moist, and concrete between depths of 350 mm – 500 mm has high moisture content. On the other hand, concrete between the outer surface of the wall and 300 mm depth in the wall is considered to have achieved a high level of drying.



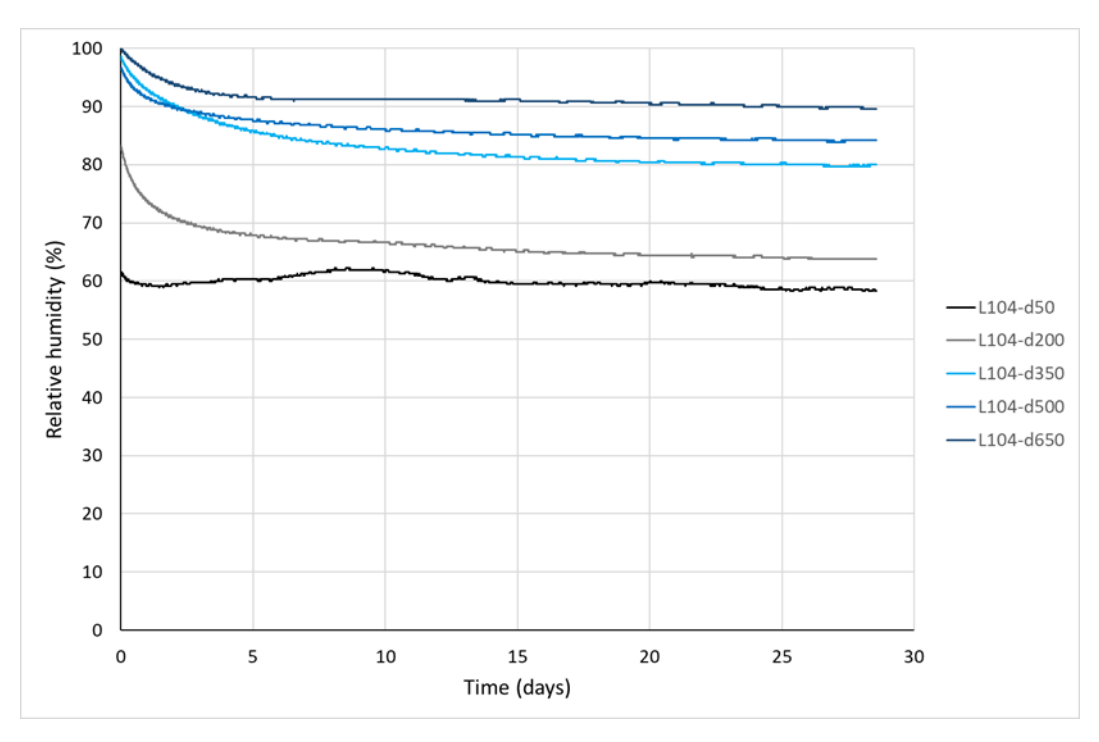


Figure 35 Results of the RH measurements on the level 104

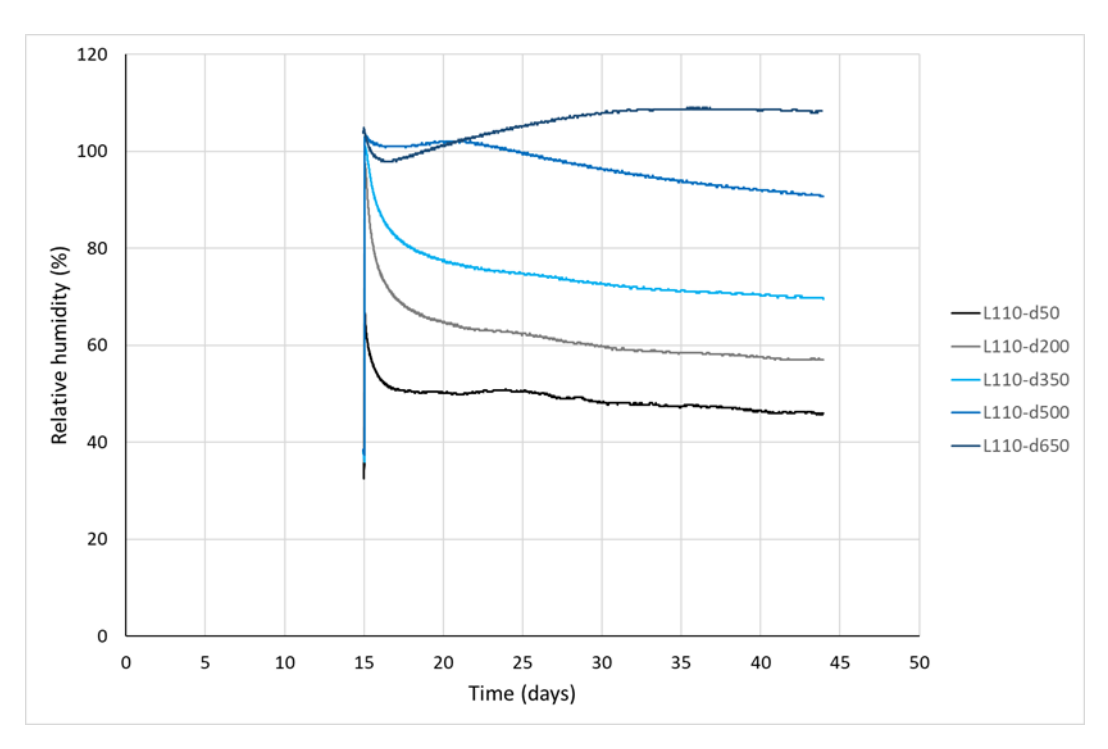


Figure 36 Result of the RH measurements on the level 110,5.



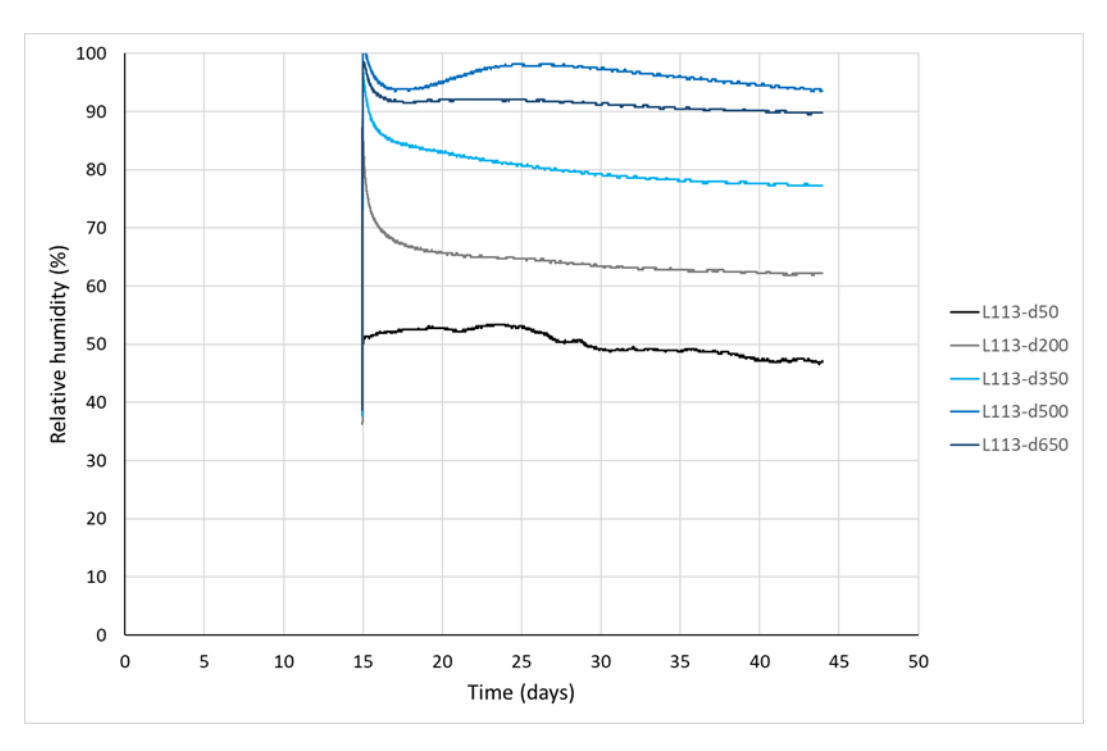


Figure 37 Result of the RH measurements on the level 113,2



## 4 Discussion and conclusions

The literature review presented in this article shows that there are different methods for determining the prestressing forces in bonded tendons. Non-destructive testing methods, which are performed without any intervention on the structure, can provide an estimate of the average prestressing force of the tendons. Non-destructive tests performed with limited local interventions are not applicable for the type of reactor containment discussed in this article. Destructive test methods based on the decompression load method cannot be applied to structures in use because the methods permanently damage the structure. The decompression test method can very well be applied to a decommissioned reactor containment, but its execution is associated with significant practical difficulties and costs. Similar destructive tests have been carried out on mock-ups of reactor containments. However, this article refers to determining the tension force of tendons through destructive testing, i.e., measuring the contraction of the tendons when they are cut.

The literature review shows that instrumentation and cutting of the prestressed strands and rods is a feasible way to estimate the reduction of their prestressing tension force. The literature review presented in this article notes prestressing force reductions between 23% and 34%. Since the reductions are determined using Hook's law, they depend on the modulus of elasticity assumed for the tendon/rod. Furthermore, the results are affected by the type of strain gauge and the manner in which it is glued to the various wires of the tendon. The strain gauge should be glued in the direction of the major principal strain direction of the wire, which is often difficult to determine. Additionally, both the wire and the strain gauge are subjected to significant stresses during the unloading process. How the accuracy of the strain gauge measurements is affected is difficult to assess.

As previously mentioned in the article, several strain gauges were mounted on the strands, and selected wires in the strands that were cut had double strain gauges. The data collected shows significant irregularities when analysing the results of individual wires/strain gauges. However, if one only considers the overall behaviour of the strand during the cutting process - the general impression seen when the results of all strain gauges on a strand are presented in a diagram - and takes into account the results of the loading of a cut strand in a testing machine, one can note a prestressing level in the strand that may very well be close to the actual prestressing level.

When the prestressing force is determined using Hook's law, the result is dependent on the assumed modulus of elasticity. This article assumes a modulus of elasticity of 195 GPa, which is lower than the values used in the referenced articles. According to the study presented in this article, the average contraction strain of the tendons is estimated to 5000 and 4000 microstrains for vertical and horizontal tendons respectively, corresponding to prestressing stresses of 975 MPa and 780 MPa respectively. The estimated contraction strains are also confirmed by the loading of cut strands in the testing machine as previously presented in the article.



The original prestressing of the tendons amounted to 1000 MPa and 800 MPa for vertical and horizontal tendons respectively, thus a prestressing reduction of 2.5% is estimated for both vertical and horizontal tendons. The prestressing reduction may seem low. This study shows that the concrete's moisture level is relatively high, which suggests that most of the concrete's shrinkage has not occurred. The low drying level also leads to lower creep in the concrete because concrete that is not exposed to drying creeps less.

The test results show that the combined effect of the adhesion between the strands and the injection grout and the friction between the strands, is sufficiently large to counteract total unloading of the strand along its entire length. After a certain distance, referred to as anchorage length, the tension in the strand rises again to the level it had before the cutting. The anchorage length has not been determined in this study but should be less than 3 meters since some windows were placed only 3 meters apart.

Cutting strands affects the strain on the concrete surfaces. With the limited number of measurement points and scanning of strain gauges that the investigation had, it is difficult to draw definitive conclusions. However, one can certainly conclude that cutting strands leads to stress changes on the concrete surfaces, and strain increase as high as 1500 microstrains can occur. This means that the concrete surface transitions from a compressed state to a tensile state. It is possible that the concrete's tensile strength has been locally exceeded.

Relatively high contraction and expansion strains were measured on the mantle of the ducts. The strains are likely due to the unloading of the strands and the stress distributions in the concrete.

According to careful visual inspections conducted, the concrete, reinforcement, ducts, and strands were in very good condition.



## 5 References

Anderson P., (2006), Thirty years of measuring prestress in Swedish nuclear reactor containments, Nuclear Engineering and Design 235, pp. 2323-2336.

Agredo Chávez, A., Gonzalez-Libreros, J., Wang, C., Capacci, L., Biondini, F., Elfgren, L., Sas, G. Assessment of residual prestress in existing concrete bridges: The Kalix bridge. To be published in Journal of Engineering Structures.

Baran, E., Shield, C., K., French, C., E., (2005). A Comparison of Methods for Experimentally Determining Prestress Losses in Pretensioned Prestressed Concrete Girders. Published in SP-231: Ned H Burns Symposium on Historic Innovations in Prestressed Concrete. 1 October 2005 Engineering, Materials Science.

Barslivo G., Österberg E., Aghili B., (2003), Utredning kring reaktorinneslutningar – konstruktion, skador samt kontroller och provningar, (in Swedish), SKI Rapport 02:58, Statens kärnkraftsinspektion (Swedish radiation safety authority), Stockholm, Sweden.

Eder, R., W., Miller, R., A., Baseheart, T., M., Swnason, J., A., (2005). Testing of Two 50-Years-Old Precast Post-Tensioned Concrete Bridge Girders. PCI Journal, May-June 2005.

Halsey, J., T., Miller, R., A., (1996). Destructive Testing of Two Forty-Year-Old Prestressed Concrete Bridge Beams. PCI Journal, September-October 1996.

Joval O., Larsson, J.-A., Lindberg T., Svärd B., Thunell B, (2002). CONMOD – Utvärdering av inneslutningen vid Barsebäck 1 Steg 1: Förberedande Strukturanalyser. Technical Report, SCTE/02401/TR-01, Scanscot Technology AB, 2002.

Naito, C., Sause, R., Thompson, B., (2008). Investigation of Damaged 12-Year Old Prestressed Concrete Box Beams. Journal of Bridge Engineering © ASCE / March/April 2008. Downloaded 05 Aug 2011 to 130.235.37.194. Redistribution subject to ASCE license or copyright. https://ascelibrary.org.

Nilsson L-O., Johansson P., (2009) Förändringsprocesser i reaktorinneslutningar, (in Swedish) Elforsk rapport 09:100, September 2009.

Pessiki, S., Kaczinski, M. Wescott, H., H., (1996). Evaluation of Effective Prestress Force in 28-Year-Old Prestressed Concrete Bridge Beams. PCI Journal, November-December 1996.

Remennnikov, A., M., Kaewunruen, S., (2015). Determination of Prestressing Force in Railway Concrete Sleepers Using Dynamic Relaxation Technique. J. Perform. Constr. Facil., 2015, 29(5): 04014134.

Roth, T., Silfwerbrand, J., Sundquist, H., (2002). Betonginneslutningar i svenska kärnkraftverk - En sammanställning över konstruktion och material. Stockholm: SKI Rapport 02:59, 2002.



Shenoy, C., V., Frantz, G., C., (1991). Structural Tests of 27-Year-Old Prestressed Concrete Bridge Beams. PCI Journal, September-October 1991.



## DETERMINATION OF STRESSES IN GROUTED STRANDS OF A REACTOR CONTAINMENT BY A DESTRUCTIVE TEST METHOD

The aim of this study is to analyze prestressed bonded tendons obtained through the decommissioning of Barsebäck nuclear power plant, to better understand the factors that influence their performance. The results show that it is possible to estimate the stress in bonded tendons through instrumentation and cutting of individual strands. Furthermore, the article shows that Barsebäck's tendons have lost remarkably little of their stress.

## A new step in energy research

The research company Energiforsk initiates, coordinates, and conducts energy research and analyses, as well as communicates knowledge in favor of a robust and sustainable energy system. We are a politically neutral limited company that reinvests our profit in more research. Our owners are industry organisations Swedenergy and the Swedish Gas Association, the Swedish TSO Svenska kraftnät, and the gas and energy company Nordion Energi.

